Urban influence on convective precipitation in the Paris region: Hectometric ensemble simulations in a case study

Arnaud Forster, Clotilde Augros, Valéry Masson

RESEARCH ARTICLE

Urban influence on convective precipitation in the Paris region: hectometric ensemble simulations on a case study

Arnaud Forster[1] | **Clotilde Augros**[1] | **Valéry Masson**[1]

[1]CNRM, Université de Toulouse, Météo-France, CNRS, Toulouse, France

Correspondence
Arnaud Forster, CNRM, Université de Toulouse, Météo-France, CNRS, Toulouse, France
Email: arnaud.forster@meteo.fr

Present address
CNRM, Université de Toulouse, Météo-France, CNRS, Toulouse, France

Funding information

The purpose of this study is to investigate the influence of the urban environment of Paris region on an isolated convective cell that formed downwind of the city on 7 May 2022, using the Meso-NH research atmospheric model at a horizontal scale of 300 m. To account for all sources of forecast uncertainty, the initial and lateral boundary conditions of the simulations are provided by the AROME-EPS ensemble prediction system. A multi-layer urban scheme is used to accurately represent the influence of buildings on the airflow. Two sets of ensemble simulations are performed: the first set (URB) uses a fine-scale surface description of the city, while the second set (NOURB) replaces urban surfaces with vegetation. This sensitivity test shows that, despite the high variability of simulated precipitation within the ensemble, the city of Paris plays a statistically significant role in the initiation of convection in this case. Convective cells are initiated over the city for several members of the URB ensemble, while almost no precipitation is simulated for the same members of the NOURB ensemble. The mean 6-hour rainfall accumulation of the URB ensemble is increased by 70% over Paris (compared to the NOURB ensemble) and no statistically significant trend is found around the city. The analysis reveals that the capital experiences a higher sensible heat flux due to drier and warmer air, resulting in enhanced vertical velocities and an increase in boundary layer height in the URB ensemble. Additionally, the total water content and cloud fraction over Paris are intensified, leading to more precipitation. These findings suggest that urbanisation has a notable impact on convection and precipitation processes in this case. **Keywords** - Urban meteorology, ensemble simulations, precipitation

1 | INTRODUCTION

Over the past few decades, the world's population has grown rapidly, and as of 2022, the Earth is home to more than eight billion people (UN, 2022). At the same time, many countries around the world have experienced a strong migration from rural to urban areas, resulting in a higher population density in cities, which cover less than 3% of the Earth's land surface but host more than half of the world's population (Grimm et al., 2008). Because of their population growth, cities are constantly evolving and attracting more and more activities such as administration, business or industry. This combination of human activities and infrastructure changes in the context of climate change makes cities more and more vulnerable to weather hazards (Masson et al., 2020). To anticipate and mitigate the consequences of climate change, it is essential to understand the meteorological processes and the interactions between the urban surface and the atmosphere (Barlow et al., 2017; Hidalgo et al., 2018).

Through the process of urbanisation (Douglas, 1983), many studies have shown that the urban environment has an impact on the local and regional climate. One of the main mechanisms of these effects is the well-known urban heat island (UHI) effect, which can alter the street canyon temperature and make the urban areas warmer than the surrounding areas (Oke, 1973; Bornstein and Lin, 2000; Tan et al., 2009). Cities can also locally affect the wind speed and the atmospheric circulation (Lemonsu and Masson, 2002; Bélair et al., 2018; Leroyer et al., 2014) and the structure of the boundary layer (Varentsov et al., 2018; Niyogi et al., 2011), which can sometimes lead to cloud persistence over the city (Theeuwes et al., 2019).

While these effects are well studied and understood, questions remain about the interactions between urban environments and precipitation. Although the community has assumed that precipitation can be modified by cities, ongoing research has not reached a consensus regarding the cities and their influences on the structure, the amount and the frequency of precipitation passing over or around them (Liu and Niyogi, 2019). In fact, due to the diversity of cities in terms of morphology, size and location, the results obtained for a specific city cannot necessarily be generalized to other cities around the world. At the same time, the variability of precipitation situations, such as thunderstorms (Bélair et al., 2018), cyclones (Zhang et al., 2018) or large-scale stratiform events (Luo et al., 2022) that may pass over a city complicates the objective analysis of the interactions between cities and precipitation (Liu and Niyogi, 2019).

More than one century ago, Horton (1921) hypothesized that a large city, such as Albany or Providence in the United States, could affect precipitation. Later in the second half of the century, Horton's hypothesis was confirmed by several studies based on the Metropolitan Meteorological Experiment (METROMEX, Changnon and Vogel, 1977) conducted in Saint Louis in the 1970s. These studies highlighted an increase in rainfall accumulation of up to 15% downwind of large cities in the United States (Huff and Changnon, 1973). More recently, there has been a rapid increase in the number of studies looking at the impact of cities on precipitation and the mechanisms involved. In a comprehensive analysis of over 400 papers on this subject, Liu and Niyogi (2019) identified general patterns in precipitation changes around urban areas: in the downwind region of the city, there is an increase in rainfall accumulation of up to 18% on average and of up to 16% over the city. This is shown by modelling case studies such as Shem and Shepherd (2009) who found an increase of up to 13% in precipitation accumulation downwind, as well as climatological studies like Kingfield et al. (2018) who showed through a radar-based analysis that megacities can increase precipitation by up to 50%.

Many investigations have been conducted to understand the urban-induced processes that alter precipitation patterns and occasionally influence thunderstorm formation. Most of them emphasize an obvious influence of the UHI which can intensify convective activity during the day (Bornstein and Lin, 2000; Shem and Shepherd, 2009). Some others pointed out that the change in boundary layer height over urban areas due to an increase in sensible heat flux can enhance turbulence and instability over the city (Guo et al., 2006; Chen et al., 2011; Shimadera et al., 2015; Zhong and Yang, 2015). At the same time, the expansion of built-up areas strengthens surface roughness, commonly referred to as the building barrier effect (Bornstein and Lin, 2000), and often leads to a decrease in upwind and an increase in downwind surface winds (Niyogi et al., 2006; Guo et al., 2006). Studies have also considered the concentration of urban aerosols above the surface, which are increased by cities and may enhance the

electrification of clouds already formed over cities (Williams et al., 1999).

While all of these processes are well understood individually, studying their interactions proves to be more challenging, as their combined effects can enhance or reduce rainfall accumulation. This complexity requires the use of a rigorous methodology to accurately distinguish and isolate random processes from clear trends in the urban influence on precipitation (Stewart and Oke, 2012; Liu and Niyogi, 2019). In literature, this impact of urbanisation is quantified using either a climatological or a modelling approach. From a climatological perspective, storms, precipitation, or lightning strikes are compared in urban areas and surrounding rural areas (Manola et al., 2020). In contrast, studies carried out with atmospheric numerical models analyse single cases (Bélair et al., 2018; Ryu et al., 2016) or multiple cases (Shem and Shepherd, 2009; Varentsov et al., 2018) where the precipitation is assumed to be modified by the city. The modelling approach is a useful tool for studying different processes at a fine scale, down to 1 km horizontal resolution in the most recent studies (Falga and Wang, 2024; Platonov et al., 2024). This allows the use of surface sensitivity tests, or atmospheric diagnostics, which help to understand surface-atmosphere interactions and dynamical or physical processes involved in the precipitation modification.

However, numerical weather prediction models are subject to various uncertainties, which impair the predictability of small-scale phenomena such as thunderstorms. In the last decade, significant progress has been made through the use of convection-permitting ensemble prediction systems (EPS, Frogner et al., 2019). These ensembles are used by operational weather forecast centres worldwide — such as WRF-based ensembles in the United States (Berner et al., 2011), MOGREPS-UK in the United Kingdom (Hagelin et al., 2017), and AROME-EPS in France (Bouttier et al., 2016). They integrate perturbations in both initial and surface conditions, as well as physics parameterisation. These prediction tools are particularly valuable in the study of convective precipitation events and their interactions with urban environments, a domain characterised by the inherently low predictability. Two recent studies focusing on Asian cities have investigated the interactions between the urban environment and the atmosphere using ensemble simulations, with and without urban surface descriptions (Zhong and Yang, 2015; Luo et al., 2022). Their ensembles consisted of different physical parametrisations, with combinations of radiation, microphysics and atmospheric boundary layer schemes. But they did not account for errors in initial conditions, surface errors or errors in large-scale boundary conditions. In this study, urban-rainfall interactions are investigated using ensemble simulations considering many sources of uncertainties in the forecast: initial and lateral boundary conditions as well as physics and surface parametrisations. To achieve this, two sets of ensembles of simulations (with and without urban description) were conducted with the Meso-NH research model, at a 300 m horizontal resolution (Lac et al., 2018). The initial and lateral boundary conditions were derived from the Météo-France ensemble prediction system, AROME-EPS. An additional pair of Meso-NH simulations was also performed using the analysis of the AROME-France numerical weather prediction (Seity et al., 2011).

The study focuses on the city of Paris as it is part of the Research and Demonstration Project for the Paris 2024 Olympic Games (RDP, 2020), which aims at advancing meteorological research in order to prepare the future 100 m resolution weather forecasting systems for urban areas. In this paper, one of the cases selected by the Paris 2024 RDP community is investigated in detail. The study of the interactions between the city of Paris and precipitation using a modelling approach is also valuable because it complements recent climatological studies. For instance, Coquillat et al. (2012) suggested an influence of the urban environment of Paris on thunderstorm and lightning activity, with an increase in the number of days with lightning strikes over and downwind of the city (based on 12 years of data). A few years later, Le Roy et al. (2020) developed a methodology to analyse rainfall accumulation and showed an increase of almost 30% in summer rainfall downwind of Paris.

The layout of this paper is as follows: section 2 describes the data used and the methodology to investigate Paris's influence on precipitation. Section 3 compares the results of the ensemble simulations with the observations and shows the differences between the set of ensembles with and without urban description. Section 4 highlights the main processes related to rainfall modification in this situation. Finally, the conclusions and perspectives are given in section 5.

2 | DATA AND METHODOLOGY

2.1 | Selected case: motivations and overview

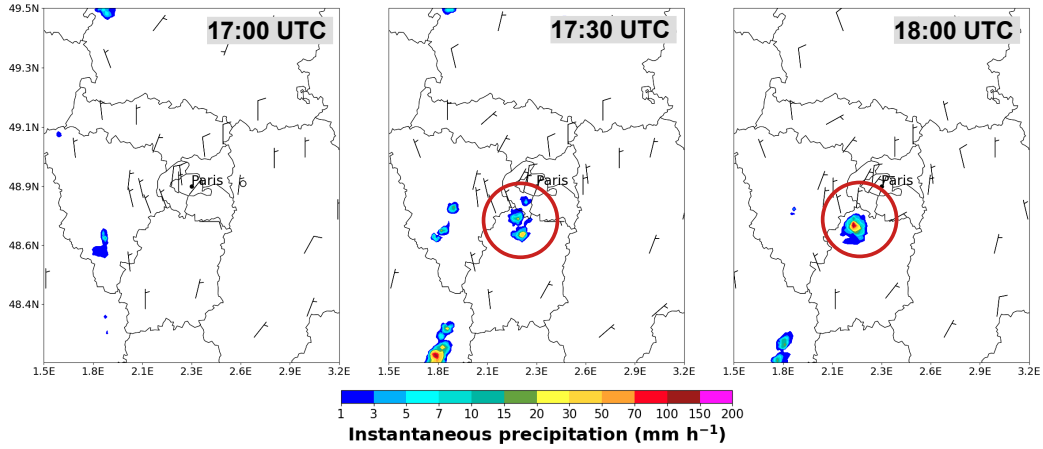

FIGURE 1 Instantaneous precipitations derived from the operational base radar reflectivity composite (see description in Figueras i Ventura and Tabary (2013)) observed over Paris region at 1700, 1730 and 1800 UTC. The red circle encompasses the thunderstorm initiation directly over and downwind of the city of Paris. The black barbs indicate the wind speed and direction at 10 m based on Météo-France operational weather stations.

On 7 May 2022, an isolated convective cell formed south of Paris, producing up to 30 mm of precipitation within two hours. Forecasters in Paris reported this meteorological event due to the north flow over Paris and the initiation of convection in the southern part of the city (i.e. downwind), which led them to assume the capital's influence on it. Although not extreme, this weather situation over the Paris region is an interesting case study to evaluate the influence of the urban environment on atmospheric convection and understand the related processes.

The city of Paris is characterised by its location along the Seine River, surrounded by hills with a maximum height of 350 m. Due to its distance from the sea, Paris experiences a modified oceanic climate, with frequent and generally mild precipitation, resulting in relatively warm summers (20.1°C) and mild winters (5.8°C), averaged over the period 1991-2020 at the Paris-Montsouris station. The climate and location of the city make it an ideal place to study the effects of urbanisation on precipitation without the influence of other geographical features such as mountains or seas (Bélair et al., 2018; Song et al., 2014).

This case study took place in spring, a season known for frequent rainfall and temperatures ranging from 10 to 20°C. On the day in question, the temperature at the Paris-Montsouris weather station was recorded as 10°C in the morning and 22°C in the afternoon. The synoptic situation was characterised by an anticyclone centred over the United Kingdom and a weak northerly flow over the Paris region. During the day, a cyclonic anomaly at 500 hPa moved from the Benelux to central France, causing a slight instability over the Paris region. Due to the high pressure remaining in the lower levels with 1024 hPa observed at Paris-Montsouris at 12 UTC, only a few convective cells developed over northern France, and one of them formed directly downwind of the city of Paris. This is illustrated in Figure 1, with the instantaneous precipitation at 1700, 1730 and 18 UTC and the wind barbs indicating a northerly flow over Paris. A convective cell was initiated directly in the southern region of Paris and reached high intensity with more than 70 mm h^{-1} at 18 UTC. The precipitation accumulation analysed between 12 UTC and

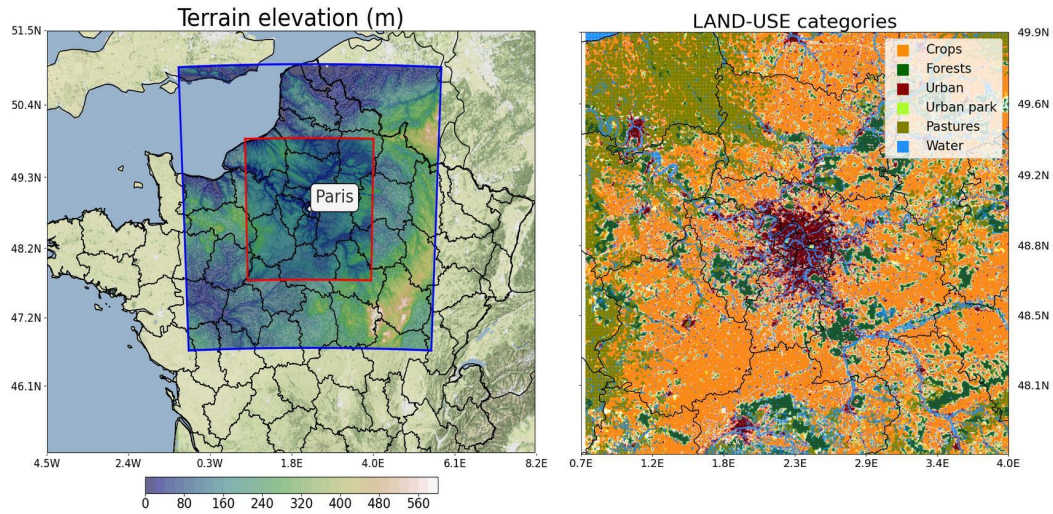

FIGURE 2 On the left is the terrain elevation for the 2 domains of Meso-NH used to compute the simulations. The coarsest domain at 1.2 km horizontal resolution corresponds to the blue domain on the map, and the red domain corresponds to the finest domain at 300 m horizontal resolution. The background of the outer surface for the left panel is provided by OpenStreetMap contributors. The land use categories in the Paris region are shown in the right panel. We can clearly see the densely urbanised area of Paris in red in the centre of the map.

18 UTC (14 h to 20 h local time) shows up to 30 mm (Figure 5) in the southern region of Paris.

2.2 | Model description

To investigate the role of the Paris urban environment in this convective case, a numerical study was carried out using the Meso-NH French non-hydrostatic mesoscale numerical model (Lac et al., 2018). This model has been used extensively to study the convection in recent years (Dauhut et al., 2015; Nuissier et al., 2020; Mandement and Caumont, 2021).

The simulation experiment uses a two-way interactive grid nesting with two domains on a limited area centred on Paris (see Figure 2). The parent domain has a 1.2 km horizontal mesh grid with a size of 480 × 480 km, while the child domain is a square of 240 km × 240 km with a 300 m horizontal resolution. The coarsest domain, which covers the northern region of France, is sufficiently large for the flow and convection to adjust to the 1.2 km mesh before it reaches the child domain. The Gal-Chen and Somerville (1975) height-based vertical coordinate is used for both domain with 90 stretched vertical levels. The first level is at 2 m and 27 levels are available between 2 and 980 m, allowing a fine description of the boundary layer. The top of the model is at 25 km, and over 15 km (the last 7 levels) a Rayleigh damping is progressively applied to the perturbations of the wind components and thermodynamic variables with respect to their large-scale values. This helps to prevent spurious reflections from the upper boundary. It has a maximum value of 0.001 $s-1$ at the top of the upper absorbing layer.

The wind transport by itself is represented by the fifth order WENO (Weighted Essentially Non-Oscillatory) scheme (Shu and Osher, 1988) combined with a fourth order Runge-Kutta time-splitting scheme (Lunet et al., 2017) for the other discretisation. The transport scheme used for meteorological (temperature, water content and turbulent kinetic energy) and scalar variables is a monotonic version of the piecewise parabolic method. These schemes are used identically for both domains. The model time step is 15 s for the coarsest grid and 7.5 s for the finest one. These small time steps are needed to keep the model stable through

the different advection schemes. To improve this stability, according to Wang and Spiteri (2007), the time step in the model is divided by 2 when the Courant-Friedrichs-Lewy (CFL) number is higher than 0.6.

In terms of physical parameterisation, the Rapid Radiation Transfer Model (Mlawer et al., 1997) is used for the longwave radiation scheme, while the shortwave scheme is based on the Fouquart and Bonnel (1980) method. Full radiation calculations are performed every 5 minutes to reduce the cost of the simulation. The aerosol distribution is extracted from the Tegen climatology (Tegen et al., 1997), a database with a horizontal resolution of $4 \times 5°$ and is not surface dependent. The microphysical scheme used here is a bulk-mixed phase one-moment scheme called ICE3 (Pinty and Jabouille, 1998; Caniaux et al., 1994). The prognostic equations predict the mixing ratios of three solid (ice crystal, snow, and graupel) and two liquid (cloud droplets and raindrops) hydrometeors. A subgrid cloud condensation scheme is also used for the parent domain to allow partial cloudiness of a grid box, providing a cloud fraction to the radiation scheme cited above.

For the turbulence, a one-dimensional parametrisation is used in the parent domain (Cuxart et al., 2000). Shallow convection and dry thermals are parametrised using a mass flux formulation, as described in Pergaud et al. (2009). In contrast, the child domain is assumed to be in the near grey zone, where most turbulence is resolved (Honnert et al., 2020). For the remaining local turbulence, a 3D turbulence parameterisation is activated. Shallow convection is assumed to be explicitly resolved, and the scheme is switched off. The model uses a mixing length adapted to every scale (mesoscale, grey zone, near grey zone and LES) to close the equations and parameterise the remaining subgrid turbulence (Honnert et al., 2021). This mixing length tends towards the one implemented by Rodier et al. (2017) for the coarsest domain, and is proportional to the horizontal grid cell size for the finest domain.

The SURFEX (SURface EXternalisée) model is used to simulate the Earth's surfaces and their interactions with the atmosphere (Masson et al., 2013). It is designed to describe surface fluxes and their evolution for 4 types of surfaces: nature, lake, ocean and city. To account for surface heterogeneity, each grid mesh is divided into four main tiles. At each time step, Meso-NH is coupled with SURFEX and several variables such as potential temperature, mixing ratio or radiation are given from the first level of Meso-NH to each mesh grid of SURFEX. In return, SURFEX calculates the momentum, sensible and heat fluxes, aerosols and other variables and returns them to Meso-NH, averaged over the four tiles.

Each tile uses a specific scheme developed in SURFEX to simulate the different fluxes over each surface. For the ocean tile, the COARE 3.0 parameterisation (Fairall et al., 2003) is implemented to represent the sea-surface fluxes. The fluxes at the air-water interface over a lake in SURFEX are calculated in a relatively simple way. It is based on the calculation of the roughness length from the Charnock (1955) formula and the parameterisation of Louis (1979) for the turbulent fluxes using a constant surface temperature of the water throughout the simulation. Regarding the natural tile, the ISBA scheme is activated with an explicit multilayer soil approach (Boone et al., 2000; Decharme et al., 2011). This approach allows the soil column to be divided into a certain number of layers, the default discretisation being 14 layers for a depth of 12 m. Finally, the TEB multi-layer scheme is implemented over the urban tile (Masson, 2000; Schoetter et al., 2020). With this new configuration, the buildings are immersed in the Meso-NH atmospheric model. This approach improves the model's results for near-surface air temperature, wind and relative humidity.

Land cover data are provided by the Ecoclimap-I Land Cover database (Masson et al., 2003) at 1 km horizontal resolution for the parent domain. This database, which gathers more than 215 ecosystems, is used in weather and climate models to define the fractions of the different surfaces present in the simulation domain (water, lakes, forests, crops, etc.) and to compute the parameters needed for surface models. The representation of the land cover in the parent domain is shown in Figure 2 with the different land use categories. For the child domain, open street map data (OpenStreetMap, 2021) are computed using the geoclimate tool (Bocher et al., 2021). They have a horizontal resolution of 100 m and provide accurate descriptions of building heights, building densities and vegetation heights.

2.3 | Ensemble of simulations design

As mentioned in the introduction, to evaluate the robustness of the results regarding the urban influence on rainfall accumulation, it is necessary to assess the uncertainties in modelling convective events. The study is based on an ensemble of 16 simulations with urban surface descriptions and 16 without. 15 of them are initialised and forced by the ensemble prediction system of Météo-France, AROME-EPS (Bouttier et al., 2016) and 1 simulation is initialised and forced by the analysis of AROME-France operational model (Seity et al., 2011; Brousseau et al., 2016) as explained in the following paragraph. These ensembles are designed to represent the major sources of uncertainty in the numerical simulation process.

2.3.1 | Input data for Meso-NH

The AROME-EPS is an ensemble based on the AROME-France numerical weather prediction system, with a horizontal resolution of 1.3 km and 90 vertical levels. It has 16 perturbed members 4 times per day (03, 09, 15 and 21 UTC) with forecasts out to times between 45 and 51 h. Each perturbed member is initiated by an ensemble data assimilation method built from explicit perturbations of the observations (Raynaud and Bouttier, 2015). The lateral boundary conditions are given by a subset of the Prévision d'Ensemble Arpège (PEARP) members, the global ensemble prediction system used at Météo-France (Descamps et al., 2014). The PEARP members used for the lateral boundary conditions are selected by a clustering algorithm (Bouttier and Raynaud, 2018). The model error is represented by a stochastic perturbation of the physical tendencies described in Bouttier et al. (2012). Surface conditions are perturbed by an autocorrelated random modification of various aspects of the SURFEX surface model (Bouttier et al., 2016).

For this experiment, the ensemble simulations start on 7 May at 09 UTC and run for 15 hours until 8 May at 00 UTC. The parent model's initial and lateral boundary conditions are provided by 15 members of the 09 UTC run of AROME-EPS every 3 hours, with a horizontal resolution of 1.3 km. Additionally, Meso-NH is initialised on 7 May at 12 UTC and forced every 3 h with the AROME analysis at 1.3 km horizontal resolution. This simulation is referred to as ARO12 in this article. It should be noted that the spin-up of the simulations was not ideal. However, the convective cells occurred around 17 UTC over Paris, which is 5 to 8 hours after the initialisation of the simulations. The use of forcing files at 1.3 km for Meso-NH helped the simulations reach equilibrium faster, reducing the spin-up time. The simulations support this statement, as ARO12 and most members of the ensemble demonstrated reasonable performance in simulating convective precipitation during the afternoon.

2.3.2 | Twin experiment: URB and NOURB ensembles

The objective of this twin experiment is to assess the potential impact of the Paris region on a typical day of diurnal convection. One approach to achieve this goal is to replace the urban scheme with the surrounding vegetation (Bélair et al., 2018; Shem and Shepherd, 2009; Luo et al., 2022). In these studies, the city is removed at the beginning of the simulations with the surface description manually modified by the authors and replaced with the most common land type in the vicinity. In our case, we used a different approach with two configurations of the Meso-NH model. The first configuration, referred to as URB, includes all the urban features described above and provides a detailed representation of the urban environment using different datasets. The second configuration, named NOURB, differs slightly from the method used in the aforementioned studies to ensure greater continuity with the files used to initialise the model. Indeed, as described by Seity et al. (2011), AROME uses the TEB scheme to describe the city. This implies fluxes modification over the urban areas, such as an increase of sensible heat flux. To prevent excessive contrast in surface variables between the initialisation files and the NOURB simulations in the first time steps, the urban fraction is gradually removed over the first two hours of the simulations. The removed urban fraction is immediately replaced by an equivalent fraction of natural vegetation. This method allowed us to simulate the effect of replacing the city with

vegetation on the surface fluxes, as described below:

$$\mathcal{F} = \mathrm{f}_n \mathcal{F}_n + \mathrm{f}_l \mathcal{F}_l + \mathrm{f}_t \mathcal{F}_t + \mathrm{f}_s \mathcal{F}_s \tag{1}$$

$$\begin{cases} \mathrm{f}_t & \rightarrow & 0 \\ \mathrm{f}_n & \rightarrow & \mathrm{f}_n + \mathrm{f}_t \end{cases} \tag{2}$$

where $\mathcal{F}$ is the total flux in the grid cell, $\mathrm{f}_{n,l,t,s}$ are the fractions of the tiles nature, lake, town and sea and $\mathcal{F}_{n,l,t,s}$ are the flux issued from the nature, lake, town and sea schemes.

In this experiment, the urban fraction is divided by 1000 over the first 2 hours of the simulations. After this replacement, the SURFEX model automatically interpolates grid points of natural cover in order to ensure a coherent natural surface cover over the Paris region. This results in a replacement of the urban surface by approximately 40% of grass, 40% of deciduous temperate broadleaf trees and 20% of crop fields.

Based on these two configurations, the URB ensemble is made by initiating and forcing the URB configuration with the 15 members of the AROME-EPS and the analysis of AROME-France. The NOURB ensemble is made by forcing the NOURB configuration with the same members. In the following sections, the URB ensemble will be called URB and the NOURB ensemble will be referred to as NOURB. A particular x member of the URB or NOURB ensemble will be referred to as mbx-URB or mbX-NOURB.

2.4 | Precipitation analysis methodology

The present study aims at evaluating the influence of the Paris metropolitan area on convective rainfall events using an ensemble analysis approach. Due to the extensive data involved, including 32 simulations, an automated method is necessary to effectively compare the ensembles and conduct a comprehensive statistical analysis of the outcomes. To meet this requirement, a new method has been developed for the Paris region, which could be extended to other large cities in the world. This method involves the evaluation of different variables, such as precipitation accumulation, temperature, humidity, and fluxes in different sectors both within and around Paris (see Figure 3).

To understand the influence of cities on precipitation in different regions, including upwind, downwind, and over the city, we focused on the area around Paris and divided it into seven distinct sectors. Each sector was analysed for precipitation accumulation and other variables within the upwind, downwind and over the city sectors. As shown in Figure 3, the central black circle with a radius of 20 km covers the entire densely urbanised part (grey background) of the region and represents the city sector. In addition, six other sectors were defined, each with an angle of 60°, extending from 20 to 60 km from the centre of Paris. These sectors were designed on the basis of previous studies (Le Roy et al., 2020; Lorenz et al., 2019), ensuring that their length (60 km radius) was sufficient to capture the influence of the city in its surroundings. The two primary sectors are the upwind sector, shown in blue, and the downwind sector, shown in red. Four additional sectors were created around these primary sectors to assess the potential impact of the city on its lateral sides depending on the wind direction. These additional sectors are referred to as the upwind left, upwind right, downwind left, and downwind right sectors.

To determine the optimal orientation of the upwind and downwind sectors, we relied on the synoptic flow data over the study area for a given time period. For each simulation, the wind orientation (based on the averaged wind between 1500 m and 3000 m) at each grid point within the large circle encompassing the 7 defined sectors was used to calculate the prevailing winds

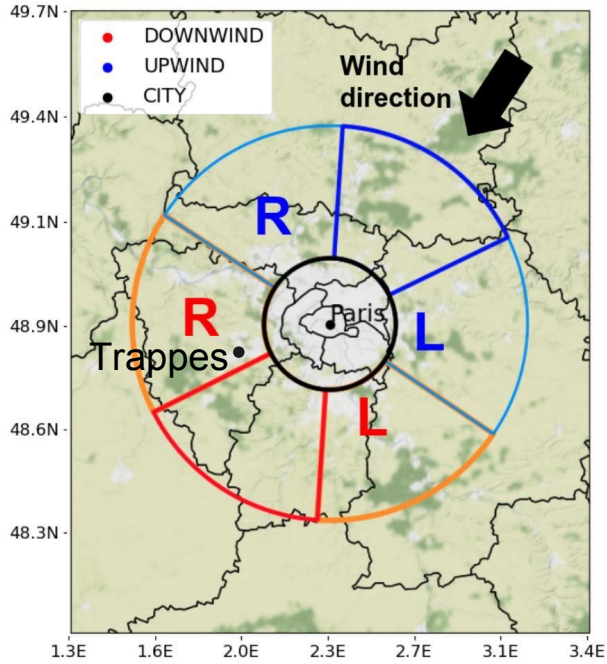

FIGURE 3 Map of the 7 sectors defined for precipitation and variables analysis. Their orientation depends on the mean wind direction in the largest circle. The blue and red sectors represent the upwind and downwind areas, while the sectors with the letters "R" and "L" indicate the left and right downwind (resp. upwind) sectors along the sides of the city. The city sector is represented by the black circle.

during the specified period. For example, in our analysis, we focused on the 6-hour rainfall accumulation to assess the influence of Paris on convective rainfall events. To do this, we calculated the average wind direction during the same 6-hour period used for the precipitation accumulation to determine the orientations of the upwind and downwind sectors.

3 | ASSESSMENT OF THE MODEL PERFORMANCE AND COMPARISON BETWEEN URB AND NOURB ENSEMBLES

3.1 | Evaluation of the model performance

In this section, the simulations of the URB ensemble at 300 m horizontal resolution are first evaluated against the observations. Statistical analyses are performed to compare the URB ensemble mean and the ARO12-URB simulation with the observations from the automatic operational weather stations of Météo-France for the following parameters: 2 m air temperature (149 stations), 2 m specific humidity (21 stations) as well as surface wind speed at 10 m (64 stations). We computed the box plots of the simulation-observation differences by extracting the ensemble mean (and the ARO12-URB simulation) at the location of each weather station in the child domain at 300 m resolution (red square in Figure 2). The box plots are displayed every hour between 12 and 21 UTC. (see Figure 4a,b,c). These times were chosen because they represent the weather situation before, during and after the initiation of convection over Paris.

The temperature at the beginning of the simulations is really well captured by the URB ensemble, with almost no difference

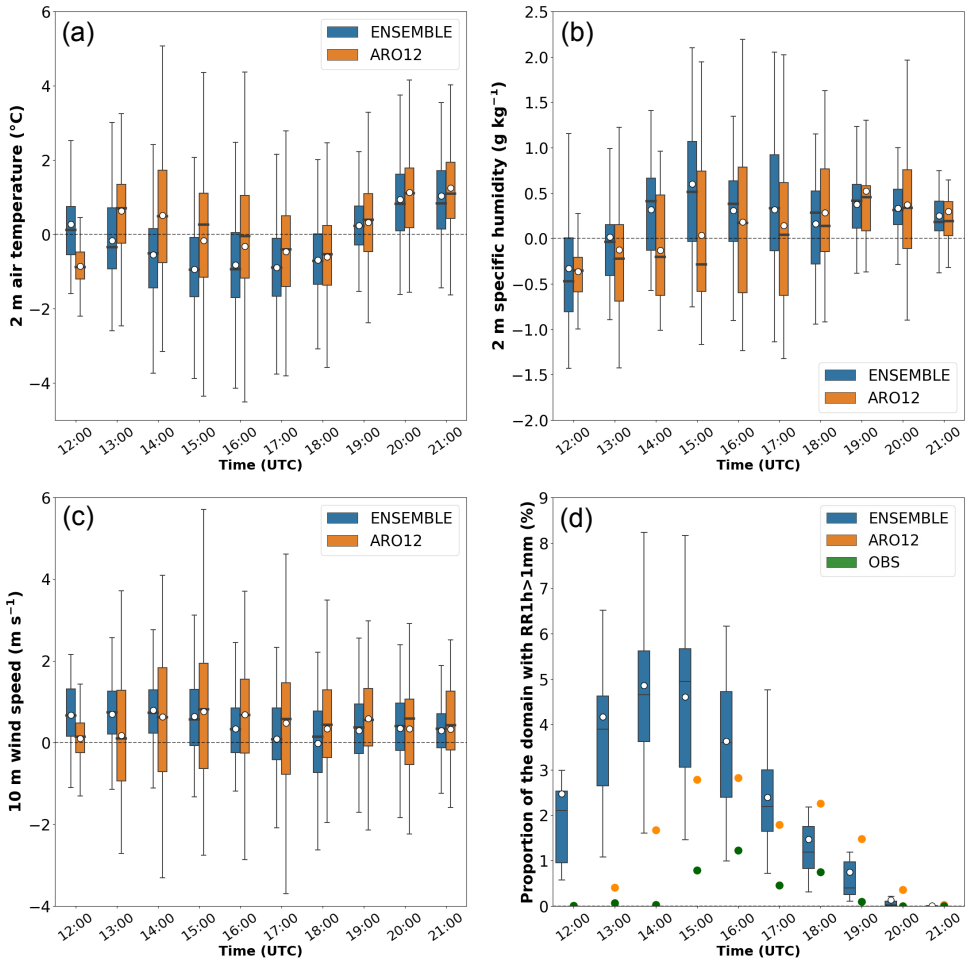

FIGURE 4 Box plots of the differences between the URB ensemble mean and observations (blue) and ARO12-URB and observations (orange) at each weather station location within the 300 m resolution child domain for (a) the 2 m air temperature, (b) the 2 m specific humidity and (c) the 10 m wind speed. Box plots are shown every hour from 12 to 21 UTC and the mean of the distribution is represented with a white circle. (d) Comparison between the URB ensemble, ARO12-URB and the ANTILOPE observations of the proportion of the child domain (in %) where hourly rainfall accumulation is over 1 mm. The data is compared on the ANTILOPE grid. The dispersion of the 15 members of the URB ensemble is represented by the box plots (blue) at each hour, and the points correspond to the values for ARO12-URB (orange) and ANTILOPE observations (green).

between the ensemble mean and the observations on average at 12 UTC. Then, Figure 4a shows that the ensemble generally has a cool air temperature bias (about 1°C) in the afternoon and a small warm bias (less than 1°C) in the evening. ARO12-URB shows initial temperature differences at 12 UTC, with lower temperatures than the observations, which could be explained by the spin-up time needed to get a more realistic feature of the atmosphere, and we can see that this is quickly corrected by the model with a small warm bias after 13 UTC and globally a good forecast accuracy in the afternoon. A warm bias is then simulated by ARO12-URB in the evening, like the one for the URB ensemble. We also note that a large spread is simulated by ARO12-URB and the ensemble in the afternoon. This can be attributed to the onset of diurnal convective precipitation in some parts of the

domain in the early afternoon, leading to a temperature decrease under the modelled precipitation that is not necessarily colocated with the observed precipitation (not shown).

The specific humidity, Figure 4b, is slightly underestimated in the early afternoon for the URB ensemble and ARO12-URB. Later, in the afternoon, the bias becomes slightly positive for the ensemble with an overestimation of the humidity of about 0.8 g kg^{-1} on average at 16 and 17 UTC. At the same time, ARO12-URB shows better forecasts of the specific humidity, with the mean of the distribution close to 0 g kg^{-1} difference. In the late afternoon and the evening, both the ensemble and ARO12-URB are slightly too humid compared to the observations. We also found on Figure 4b that the variability within the simulations at the observing sites is larger in the afternoon, as for temperature. This is mainly due to diurnal convection leading to precipitation in some parts of the domain (either in the simulations or in the observations), which locally increases the specific humidity. The wind speed is well simulated by both the ensemble mean and ARO12-URB. Throughout all the time steps, the simulations show a small positive bias, with a median difference of 1 m s^{-1} in the afternoon and less than 1 m s^{-1} in the evening.

To visualise the performance of the 300 m simulations in forecasting precipitation timing and intensity, we calculated the proportion of the child domain where the hourly rainfall accumulation for the URB ensemble (blue) and ARO12-URB (green) are over 1 mm (see Figure 4d). This was compared with the fraction observed (green) from the ANTILOPE (ANalyse spaTiaLisée hOraire des PrEcipitations) quantitative precipitation estimate (QPE) algorithm (Laurantin, 2013). This algorithm combines rain gauges and radar measurements to spatialise rainfall accumulation with a horizontal resolution of 1 km. The simulations were interpolated to the ANTILOPE grid to compare the results at each point of the domain every hour between 12 and 21 UTC. It should be noted that the hourly rainfall accumulation for ARO12-URB is not available at 12 UTC due to the simulation starting at that time. In Figure 4d, we see a clear overestimation of the proportion of the domain with hourly rainfall over 1 mm for the simulations, especially in the early afternoon, for the URB ensemble and slightly less for ARO12-URB. The observations indicate that the precipitation on this day was confined to a small part of the domain, as no more than 2% of the child domain is covered with hourly rainfall over 1 mm. Although the difference between simulations and observations is large on the graph, it only reaches a maximum of 5% between the URB mean and the observations on this day, at 14 UTC. This seems reasonable, when one considers the small fraction of the domain concerned by precipitation in both the simulations and the observations.

To complete the study of the performance of the simulations for the precipitation representation, we calculated the 6-hour rainfall accumulation (12-18 UTC) for each member and compared them with the rainfall observations from the ANTILOPE data (Figure 5). We observe a clear overestimation of the amount of precipitation in the Meso-NH simulations compared to the observations. Only a few precipitation accumulation patches are observed in the Paris region during this period, with the main one located in the south of Paris, possibly initiated by the city. The simulations show considerable variability, characterised by distinct precipitation patches for each member. In particular, two distinct clusters are visible: one with lower precipitation accumulation for members 3, 4, 12, 13 and 15, as well as for ARO12. On the other hand, the remaining members show more widespread and higher rainfall accumulation.

The diversity in the forcing data explains the variability in the simulations. In our study, we used the 09 UTC run of the AROME-EPS forecast, and at first sight we noticed an overestimation of precipitation in most members of the operational ensemble. Therefore, it is reasonable to observe a similar trend in the meso-NH simulations.

To better understand the high variability within the ensemble, a comparison was conducted using the available radiosounding data from Trappes, located west of Paris (see Figure 3). In Figure 6, the observed profiles (thick black curves) obtained on 7 May at 12 UTC, are compared with the simulated profiles of potential temperature and specific humidity calculated as horizontal averages within a 10 km window around Trappes to smooth the variability of the variables. The plots show a significant variability of the profiles across the ensemble. The simulated potential temperature ranges from 16°C to 20°C near the surface (for an observed temperature of 17°C), while the specific humidity generally appears to be lower than the observations for most ensemble members at the lowest altitudes (below 1000 m AGL). To provide a simple estimate of the height of the boundary layer, we examined the change in the variation of the potential temperature in the vertical direction. The lowest points of the sharp rise

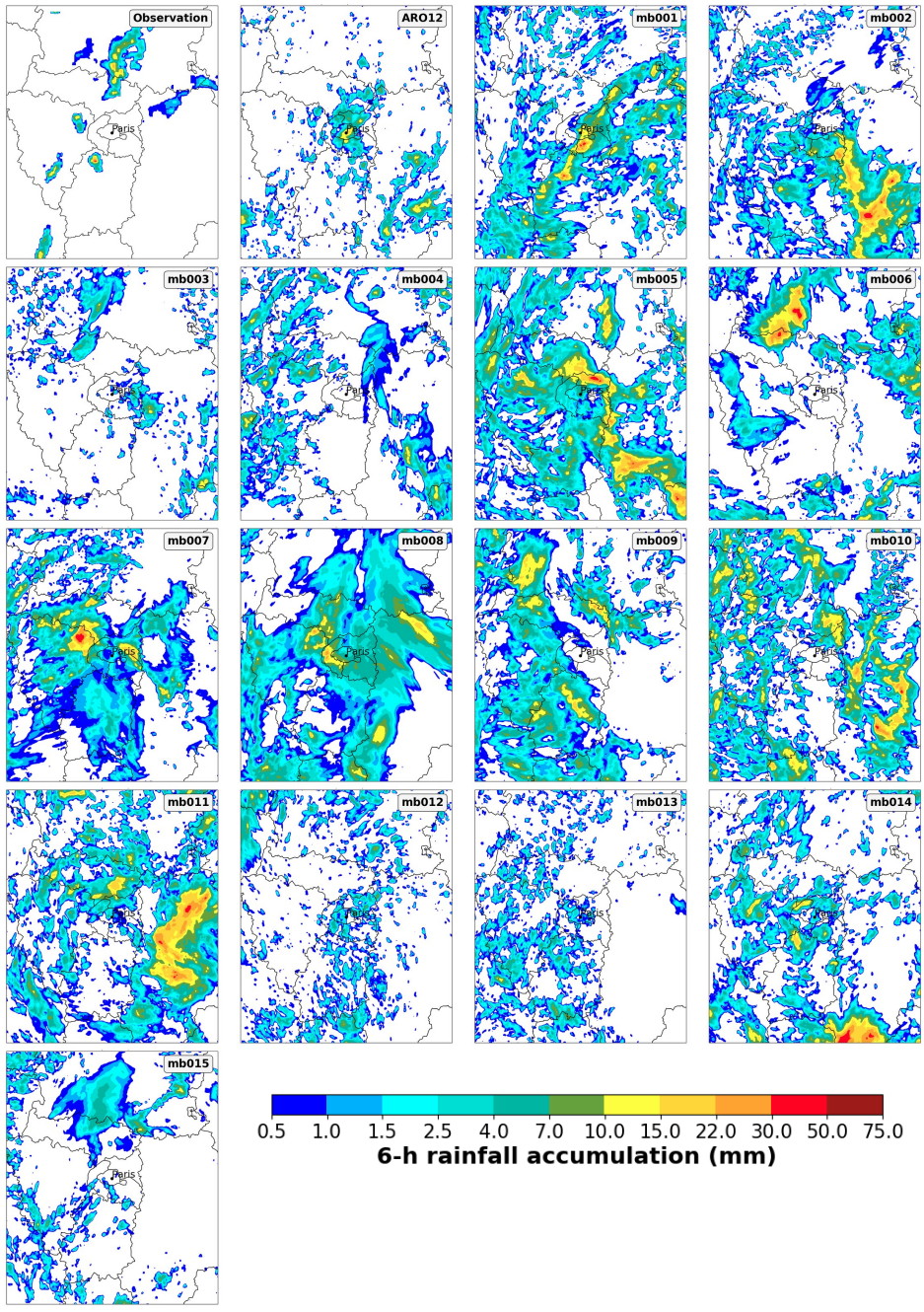

FIGURE 5 Maps of the 6 h rainfall accumulation (from 12 to 18 UTC) observed in the ANTILOPE analysis or simulated in all URB simulations: ARO12-URB and the 15 URB simulations forced by AROME-EPS members.

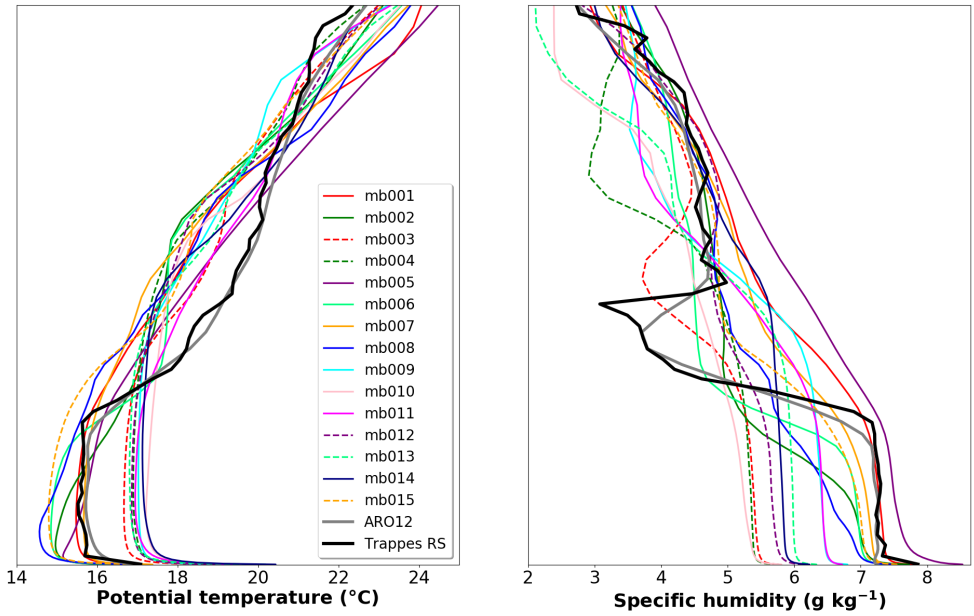

FIGURE 6 Vertical profiles of the potential temperature (left) and specific humidity (right), observed by Trappes radiosounding and calculated as horizontal averages within a 10 km window around Trappes for all URB simulations (members 1 to 15) and ARO12-URB simulation. The dashed lines correspond to the less precipitating simulations from the URB ensemble: members 3, 4, 12, 13 and 15.

in temperature, depicting an inversion, were selected as the boundary layer height. Looking at the radio sounding, this simple method indicates that the boundary layer height is situated around 900 m, while within the ensemble, this height varies between 400 m and 2000 m, depending on the member. This further illustrates the high variability within the ensemble, with two distinct clusters: one characterised by colder temperatures and a shallow boundary layer, and another with warmer temperatures and a higher boundary layer. These two clusters help to explain the observed differences in precipitation accumulation within the ensemble. In Figure 6, we highlight the members with low precipitation accumulation according to Figure 5 using dashed lines. Among four out of five members with low precipitation, the potential temperature in the lower levels appears warmer compared to the observations, and the boundary layer, in general, is more developed. Simultaneously, the vertical profiles of specific humidity indicate a drier atmosphere for these four members. With this dry air, convection does not initiate in the larger domain, as it does for the more humid members. For the remaining member with low precipitation accumulation, the atmosphere may have been too cold to initiate convection.

The ARO12-URB is initialised at 12 UTC using the AROME analysis, which includes the radiosounding in the assimilation process. As a consequence, it is normal to see a better agreement between the ARO12 simulation and the observations. This can explain the better precipitation results shown in the previous paragraph for this simulation.

The use of an ensemble usually implies a high variability within the results. Due to the non-linearity of the equations, we know that small changes in the initialisation, forcing or parameterisation of the equations can lead to large differences in the results. This is exactly what the ensemble illustrates for the 7^{th} of May situation. However, the main objective of the study is not to evaluate the accuracy of the forecasts, but to consider all uncertainties in the modelling and assess the urban impacts on precipitation.

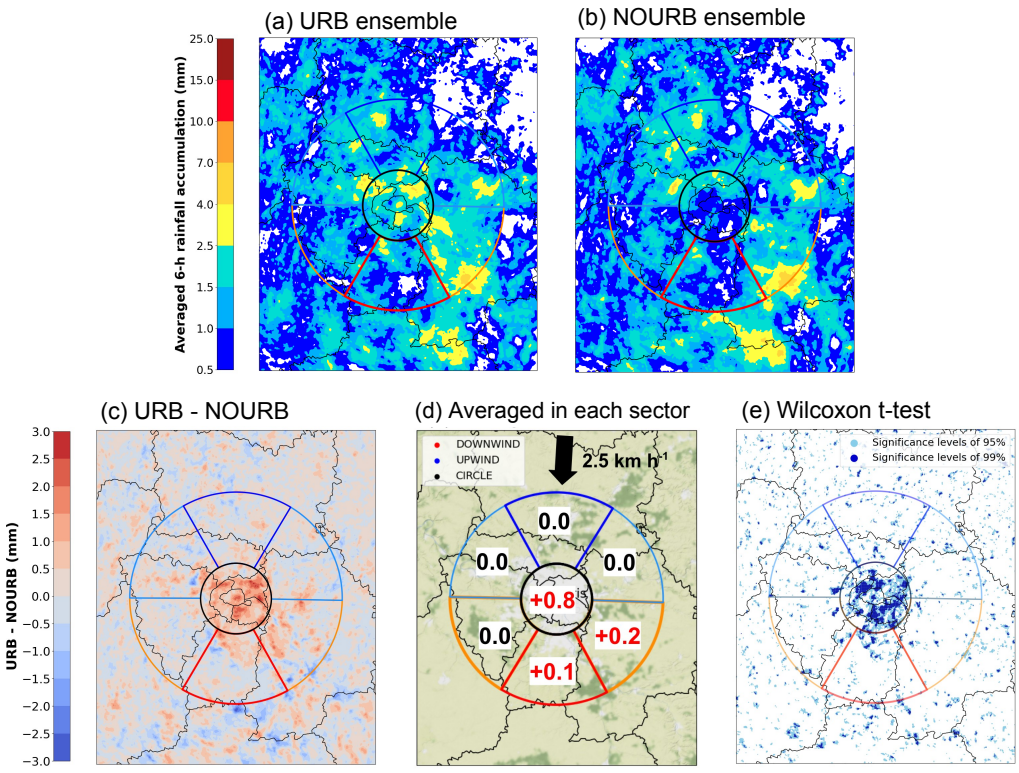

FIGURE 7 (a) Ensemble mean 6 h precipitation accumulation (12-18 UTC) for the URB ensemble, and (b) for the NOURB ensemble. (c) Difference between the URB and NOURB ensembles for the 6 h accumulated precipitation. (d) Average precipitation accumulation difference computed in each sector. (e) Results of the Wilcoxon t-test of statistical significance for URB - NOURB shown in (c), with cyan and dark blue colours indicating significance levels of 95% and 99% respectively.

3.2 | Comparison between URB and NOURB ensembles

To evaluate the effect of the urbanised area of Paris on the convection, the URB and NOURB ensembles are compared for the simulated rainfall accumulation. The averaged precipitation over 6 hours between 12 and 18 UTC is shown in Figure 7a for the URB ensemble and Figure 7b for the NOURB ensemble. Both ensembles consist of 16 members. On average, precipitation patches are relatively similar between the URB and NOURB ensembles, except within the city sector over Paris where rainfall accumulation is lower in the NOURB ensemble. This is clearly shown with the difference between the URB and NOURB ensembles in Figure 7c with a red zone over Paris region. We also observe negative areas in other parts of the domain, but they are often next to areas with positive values: they reflect a slight shift in precipitation between URB and NOURB simulations, resulting in a precipitation dipole. Averaging the precipitation accumulation difference within each sector gives an average increase of +0.8 mm in the URB simulations over the city of Paris and an increase of +0.2 mm downwind of the city (Figure 7d. These results are consistent with previous studies reporting increased precipitation over urban areas (Shem and Shepherd, 2009; Bélair et al., 2018). Although these 6-hour rainfall accumulation differences between URB and NOURB are relatively small (never exceed 4 mm in Figure 7c), the mean increase of +0.8 mm over the city corresponds to a 70% relative increase in precipitation, which is notable.

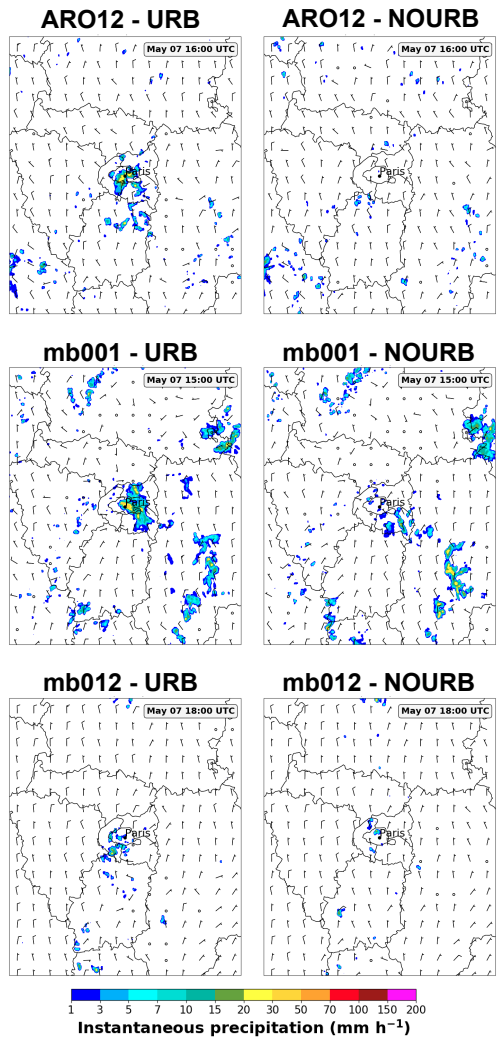

FIGURE 8 Instantaneous precipitation and wind barbs at 10 m at the peak of the precipitation intensity for the URB members. URB simulations are on the left and NOURB are on the right. ARO12 is at the top, and members mb001 and mb012 are in the middle and bottom, respectively.

To better understand the differences in mean precipitation accumulation between URB and NOURB, we selected a number of twin simulations (URB vs. NOURB configuration) where the URB members are quite close to the observations. It is important to note that in such a situation of diurnal convection, it is very difficult to simulate the correct timing and location of convective cells. Here, we examine the twin simulations when the instantaneous precipitation rate over the city is maximum. The results are displayed in Figure 8 for 3 members of the ensembles. In the ARO12-URB simulation, convection is initiated over the city, with the peak intensity reaching 20 mm h^{-1} at 16 UTC, while no precipitation is simulated over Paris in ARO12-NOURB. Convection is also initiated in mb001-URB and mb012-URB with peak intensities at respectively 15 UTC and 18 UTC respectively, while

almost no precipitation is simulated in the corresponding NOURB simulations. An in-depth study of the processes is proposed in section 4 to better understand the role of the Paris environment in the initiation of the precipitation event on 7 May 2022.

3.3 | Robustness of the results

To ensure that the results obtained for Paris and its environs were significant and confirmed an increase in precipitation over the city, several tests were conducted.

For the first test, we computed simple statistics on the differences between the URB and NOURB ensembles in each sector. The median, the mean and the 90^{th} percentile were calculated for each ensemble and are shown in the Table 1. Over the city we find an increase of up to 0.85 mm for the mean and more than 2 mm for the 90^{th} percentile. In the other sectors, almost no differences are found, except in the downwind left sector where an increase of 0.2 mm is found for the mean of the URB ensemble.

TABLE 1 Statistics on the URB - NOURB 6h precipitation accumulation differences in each sector (mm).

Sector	Mean	Median	90^{th} percentile
City	0.85	0.38	2.22
Downwind left	0.20	0.04	0.64
Downwind right	-0.03	0.0	-0.05
Downwind	0.04	0.05	0.22
Upwind left	-0.02	-0.02	-0.11
Upwind right	0.03	0.0	0.15
Upwind	-0.03	-0.01	-0.08

A second statistical test was performed over the Paris region using a Wilcoxon-Mann-Whitney rank-sum test (Wilks, 2006). The test was applied to the accumulated precipitation over 6 hours at each grid point of the URB and NOURB ensembles, respectively. The results on the domain are shown in Figure 7e. The cyan and dark blue colours indicate areas where the differences between the URB and NOURB ensembles are statistically significantly different, at a confidence level of 95% and 99%, respectively. The results show that the areas with positive precipitation anomalies in the city sector (Figure 7c) are also the areas with statistical differences between the two ensembles. This illustrates the robustness of the precipitation response from urbanisation in this case.

A final statistical test was performed to ensure the robustness of the results in each sector (Figure 7d). As the experiment was limited to 16 members for the URB ensemble and 16 for the NOURB ensemble, we artificially increased this number using the bootstrap method (Efron and Tibshirani, 1993). This technique, based on resampling with replacement, allows the calculation of the confidence intervals of a dataset. In this case, it is applied to the average of the URB and NOURB ensemble differences for the 6-hour rainfall accumulation in each sector (see Table 2). After resampling the URB-NOURB dataset 10000 times, we observe an average increase in precipitation of 0.85 mm in the city sector for URB compared to NOURB ensemble. Based on a confidence level of 95%, the confidence interval ranges from 0.52 to 1.21 mm, confirming a statistically significant increase in precipitation over the city for the URB ensemble. In the other sectors, except downwind left, the confidence intervals are almost centred on 0, meaning that no significant differences are simulated by the ensembles. In the downwind left sector, a mean increase of 0.2 mm is simulated with a confidence interval ranging from 0.0 to 0.44 mm, confirming also a slight increase in precipitation downwind left of the city.

TABLE 2 Bootstrapping on the sample of URB-NOURB accumulated precipitation differences (mm) averaged within each sector. The confidence interval is based on a confidence level of 95%.

Sector	Mean	Confidence interval
City	0.85	[0.52, 1.21]
Downwind left	0.20	[0.0, 0.44]
Downwind right	-0.02	[-0.17, 0.11]
Downwind	0.04	[-0.1, 0.19]
Upwind left	-0.02	[-0.11, 0.04]
Upwind right	0.03	[-0.06, 0.13]
Upwind	-0.03	[-0.1, 0.02]

4 | DISCUSSION: ROLE OF THE URBAN ENVIRONMENT

The quality of the modelling results discussed in the previous section is influenced by various factors. These factors include the horizontal resolution of the model, the initial atmospheric conditions, the surface forcing, and the representation of specific physical processes such as cloud microphysics, implicit or subgrid-scale convection, and boundary layer mixing. The use of an ensemble allows us to observe the variability in the modelling of the situation, depending on the quality of the ensemble. It also allows us to identify the most influential factors that contribute to significant differences between the URB and NOURB ensembles or within a twin experiment. In this study, we focus on the analysis of the key variables related to the urban environment that could contribute to the observed increase in rainfall accumulation over Paris. However, it is important to note that the differences between the URB and NOURB ensembles may be relatively small compared to the differences found between individual members within the ensemble.

4.1 | Warmer and drier atmosphere over Paris

Special attention was given to the near-surface region to evaluate changes in the following variables: 2 m air temperature, 2 m specific humidity and latent and sensible heat fluxes. The temporal evolution of the ensemble mean and dispersion for each variable was analysed within the city sector, which exhibited the most significant differences between URB and NOURB.

When examining the temporal evolution of the temperature displayed in Figure 9a, an increase in the mean of the URB ensemble (red curve) is clearly visible. The gap between the URB and NOURB ensembles becomes more pronounced after 10 UTC as the TEB urban scheme is progressively removed. This is an illustration of the urban heat island effect, which leads to a temperature increase (in URB compared to NOURB) of about 1°C during the day and more than 2°C during the following night over the Paris region. These results are in good agreement with previous studies carried out in Paris, which reported an average urban heat island effect of less than 1°C during the day and about 2.5°C during the night (Le Roy et al., 2020). On Figure 9b, we can see the urban footprint on the temperature at 13 UTC, just before the convection starts in most of the simulations. The positive anomaly depicts an increase of temperature for the URB ensemble, and the highest differences are located in the centre of Paris and in the south of the capital. The spread of the ensembles shown in the temporal evolution (Figure 9a) also highlights the high variability we already observed earlier, with differences of more than 4°C between the coldest and the warmest simulation in the ensemble. This is mainly due to the formation of showers over Paris in the simulations, which occurred earlier in some simulations Figure 4. In the 7 May case, the urban heat island effect is not particularly intense due to lower daytime heating and

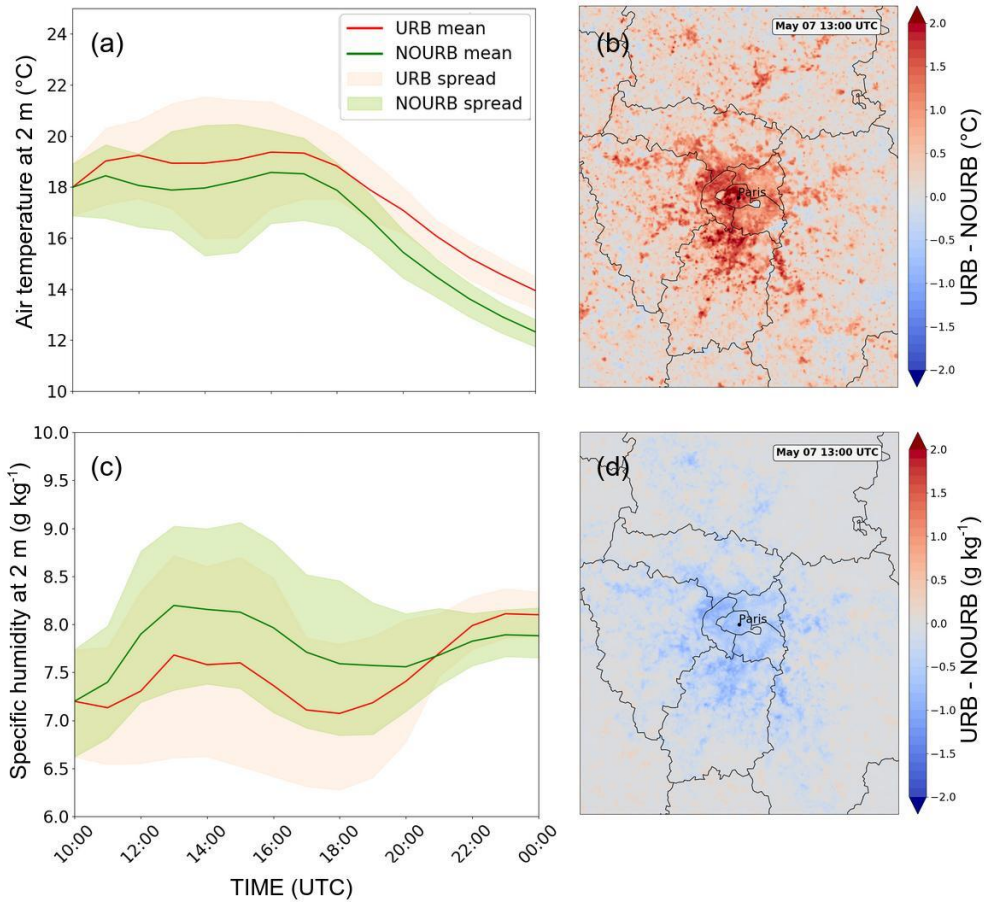

FIGURE 9 Time series of the URB and NOURB ensemble mean of (a) 2 m temperature and (c) 2 m specific humidity, averaged in the city sector. The intervals between 10th and 90th percentiles are represented by shaded colours. Difference between URB and NOURB ensemble means at 13 UTC for (b) the 2 m air temperature and (d) 2 m specific humidity.

radiation. On average, the temperature for the hottest simulation in the URB ensemble over Paris only reaches 22°C, and the radiation is not at its maximum due to the different convective cells passing over Paris.

Another effect of the urban environment within the ensembles is simulated in the specific humidity at 2 m (Figure 9c). Due to the predominance of impervious materials and the low density of vegetation in Paris, the water availability is reduced, leading to lower humidity in the urban environment during the day (Hage, 1975). This is evidenced by a lower 2 m specific humidity in the URB ensemble during the day. At 13 UTC, the areas with lower specific humidity in the URB simulations (Figure 9d) correspond well with those classified as "urban" in the land use map shown in Figure 2. In general, the NOURB ensemble simulates on average specific humidity values of about 8.3 g kg^{-1} in the afternoon before the convection initiation, while the URB ensemble shows an average of only 7.7 g kg^{-1}. The high variability, represented by the spread of the ensemble in the graphs, highlights the differences between the individual members. In fact, the ensemble simulates different weather conditions, with small showers, heavy rain or dry weather during the afternoon. This leads to a high variability of the humidity over Paris as well as for the temperature at 2 m. However, the general trend is confirmed in the URB ensemble, with a drier atmosphere

over Paris during the day. This trend is consistent throughout the entire simulation, except during the night, when the specific humidity is slightly higher in the URB ensemble compared to the NOURB ensemble. This may seem counterintuitive at first, as Paris has a relatively low vegetation cover compared to the surrounding areas. But nighttime temperatures are warmer in the city (UHI) and allow for higher humidity, with steam further from saturation, leading to less water loss by condensation (Hage, 1975; T. R. Oke, 2017).

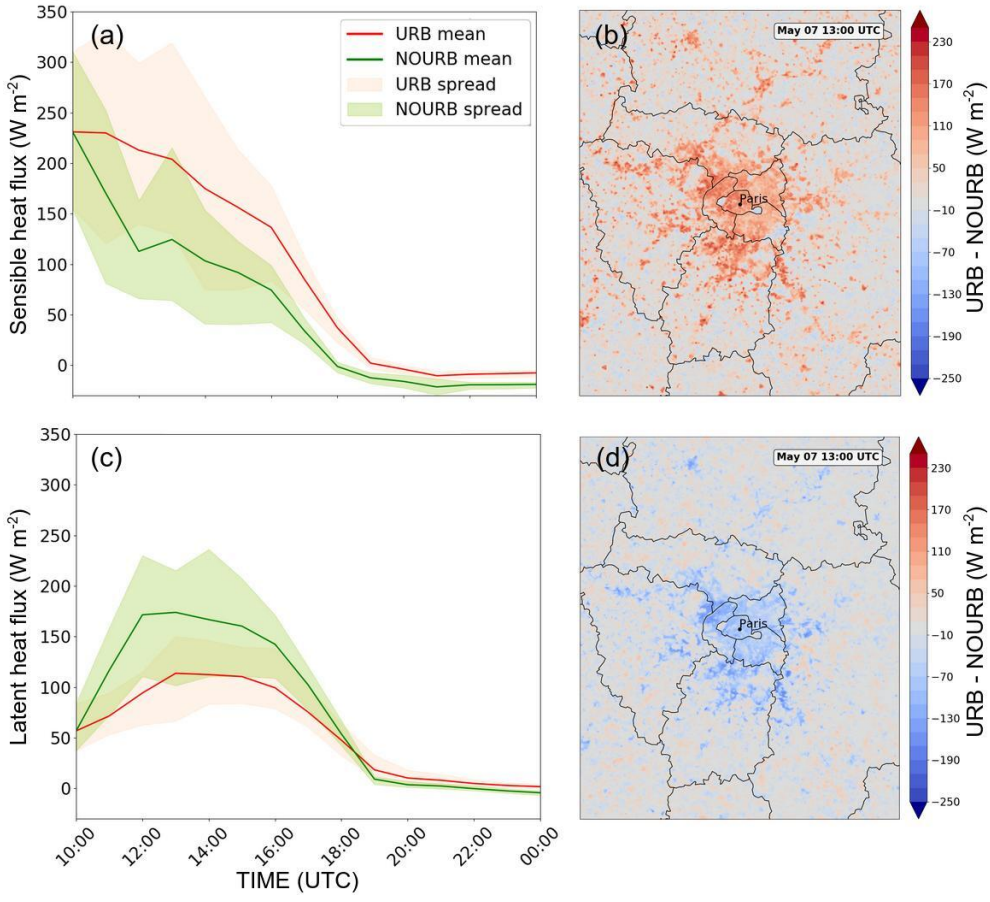

FIGURE 10 Same as Figure 9 for the sensible heat flux (a) and (b), and for the latent heat flux (c) and (d).

A well-known consequence of warmer surfaces and drier air in the urban area is an increase in the sensible heat flux (Guo et al., 2006; Bélair et al., 2018) and a decrease in the latent heat flux due to less vegetation in cities and limited evaporation processes (Lemonsu and Masson, 2002). This phenomenon is well simulated throughout the day, with a significant difference in the fluxes between the URB and NOURB ensembles (Figure 10a,c). At 13 UTC, the sensible heat flux in the URB simulations is almost 100 W m^{-1} higher in the centre of Paris (Figure 10b), and the URB-NOURB difference is positive over a large area where the urban surfaces are present. Conversely, the latent heat flux over the Paris region is lower in the URB simulations (see blue negative values in Figure 10d with a difference of up to 100 W m^{-1} in the north-west of Paris).

Figure 10a and Figure 10c also depict the temporal evolution of the ensemble mean and the dispersion within the city sector

for the sensible and latent heat fluxes. We observe that the sensible heat flux averages about 230 W m^{-2} at the beginning of the simulation. As we gradually remove the urban area at 10 UTC, the differences between the URB and NOURB ensembles steadily increase, reaching a maximum difference of 90 W m^{-2} on average at 12 UTC. Throughout the day, the difference between URB and NOURB remains positive, indicating that more sensible heat flux is generally available in the URB simulations. Conversely, the latent heat flux is generally higher for the NOURB ensemble, with a maximum difference of about 60 W m^{-2} during the afternoon. This can be attributed to the significant decrease in moisture availability over urbanised areas, as indicated by the specific humidity discussed in the previous paragraph. The results show a high variability, strongly influenced by clouds and showers over Paris in the afternoon, but the overall shift towards higher values of sensible heat flux and lower values of latent heat flux in the URB ensemble is significant. This confirms the influence of the Paris urban environment on the near-surface variables.

4.2 | Effect of the urban environment on vertical velocities and boundary layer height

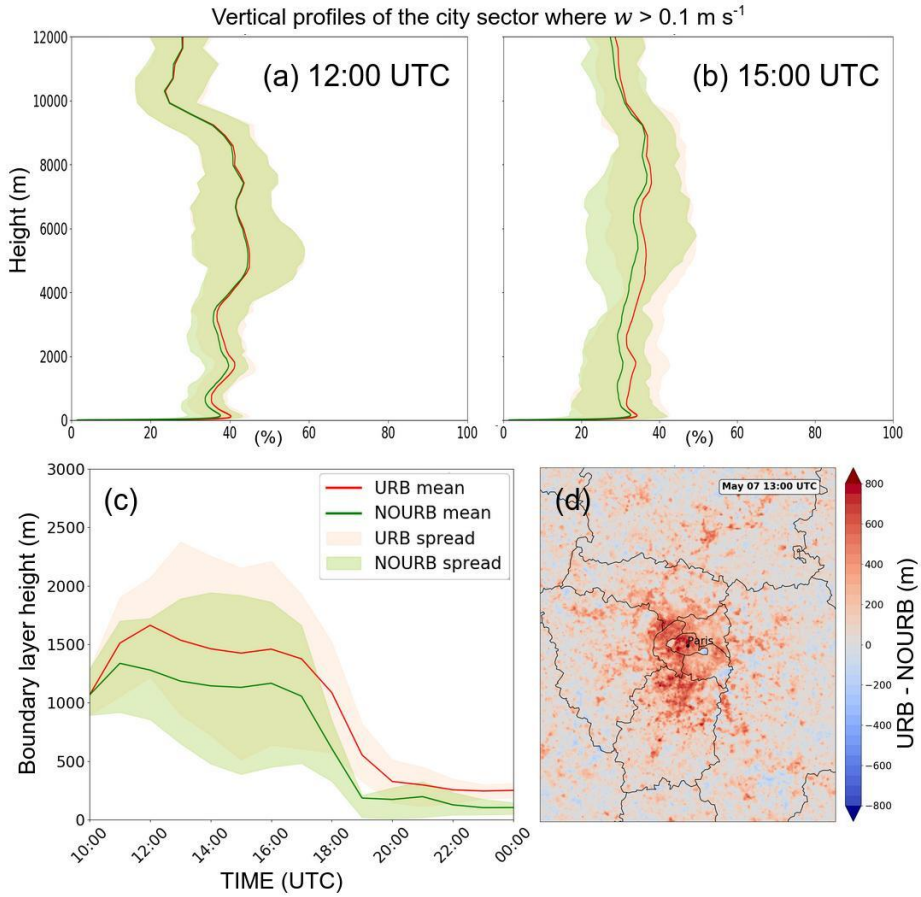

FIGURE 11 (a,b) Vertical profiles of the percentage of the city sector where the vertical velocity is over 0.1 m s^{-1} at 12 UTC, and at 15 UTC. (c) Time series of the boundary layer height from the URB and NOURB ensembles, averaged in the city sector. (d) Boundary layer height difference between URB and NOURB ensembles at 13 UTC.

Several articles have shown that the vertical velocities can be increased above the urban environment (Niyogi et al., 2011; Zhong and Yang, 2015). The percentage of the city sector with vertical velocities over 0.1 m s^{-1} for each level of the model is shown, at 12 UTC in Figure 11a and 15 UTC in Figure 11b. This diagnostic highlights the percentage of updrafts simulated in each ensemble. A difference between the two ensembles is visible in the early afternoon near the surface: at 12 UTC a larger part of the domain of the URB ensemble has vertical velocities over 0.1 m s^{-1} than in the NOURB ensemble. This difference propagates in the upper levels and increases in the afternoon. At 15 UTC, over Paris, the surface area with positive vertical velocities is larger for the URB ensemble than for the NOURB ensemble in the entire column of the model (Figure 11b). Up to 8000 m, the URB ensemble consistently contains a 2 to 5% larger surface area with positive vertical velocities than the NOURB ensemble. This can be explained by the enhanced sensible heat flux over urban surfaces, which increases the vertical velocities over Paris in the boundary layer, and as a consequence, the vertical velocities are also increased in the higher atmosphere.

At the same time, an estimate of the boundary layer height was computed on the simulations, using the bulk Richardson method (Richardson et al., 2013), to assess the modification of the atmosphere induced by the urban environment. The time series of the averaged boundary layer height for each ensemble is shown in Figure 11c, and the difference between the two ensembles at 13 UTC is displayed in Figure 11d. Both figures illustrate a greater boundary layer height when the urban areas are included. This is a direct consequence of the higher sensible heat fluxes and stronger vertical velocities over the Paris region. The boundary layer is 200 to 300 m higher for the URB ensemble during the day and 100 to 200 m higher during the night. At 13 UTC, the boundary layer height difference between the URB and NOURB ensembles reaches more than 700 m in the city centre, showing a strong effect of the dense urban area on the boundary layer development (Niyogi et al., 2011; Rozoff et al., 2003).

4.3 | More clouds and water available over the city

In a cloud-resolving model, the cloud fraction is calculated for each grid cell, ranging from 0 to 1. A fraction greater than 0.5 indicates the formation of cumulus and thicker clouds, such as cumulonimbus. By comparing the percentage of the city sector where the cloud fraction exceeds the threshold of 0.5 in both ensembles (Figure 12a,b), we can observe the effects of increased updrafts and a higher boundary layer height on cloud formation. Indeed, with stronger vertical velocities and a higher boundary layer in the URB ensemble, particles have a greater chance of reaching the lifting condensation level, which is a good approximation of the cloud base (Markowski and Richardson, 2010). In the simulations, we observe an expansion of the cloud cover over Paris in the URB ensemble starting around 12 UTC in the lower atmosphere and spreading to the higher levels in the afternoon. Around 15 UTC, just before the onset of thunderstorms in most simulations, the city sector has 4 to 5% more points where the cloud fraction is over 0.5 for URB than NOURB ensemble. This finding is consistent with the results of Theeuwes et al. (2019) over Paris, who reported a 5 to 10% increase in cloud fraction compared to the surrounding areas during summer afternoons. However, it is important to note that there is a considerable variability in these cloud-related variables. At 15 UTC, the 10^{th} percentile indicates that, on the whole column, only 5% of the city sector is covered by a cloud fraction over 0.5. But at 6000 m, nearly 80% of the city sector has a cloud fraction over 0.5 in the 90^{th} percentile for URB and NOURB ensembles. This variability is strongly dependent on the simulated weather conditions. Some members may have already formed clouds over Paris, resulting in high cloud fractions, while others may have formed showers later, leaving the sky relatively clear at 15 UTC. Nevertheless, the ensemble trend suggests an increase in cloudiness over Paris. It is also interesting to note that the variability of the ensemble serves as a reminder of the challenges in accurately simulating fine-scale phenomena such as convective clouds.

However, it is important to note that an increase in cloud cover does not always result in an increase in precipitation accumulation. In Figure 12c, we compared the total amount of liquid and ice water per cell in the air column from cloud base to top height, known as the liquid and ice water path. On average, in the city sector, the URB ensemble shows higher values of the total liquid and ice water path compared to the NOURB ensemble. The peak occurs in the afternoon, around 13 UTC, with values reaching up to 260 g m^{-2} for the URB ensemble, compared to 210 g m^{-2} for the NOURB ensemble. This represents

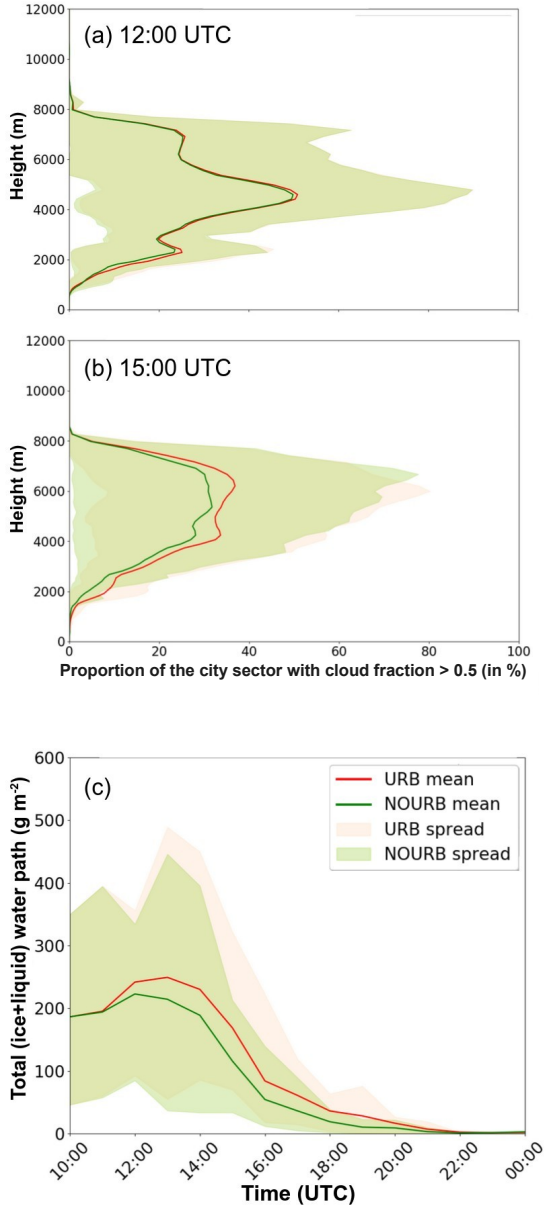

FIGURE 12 (a,b) Vertical profiles of the percentage of the city sector with cloud fraction > 0.5 at 12 UTC and 15 UTC. (c) Time series of total (liquid+ice) water path averaged within the city sector for URB and NOURB ensembles. The intervals between 10th and 90th percentiles are shown with shaded colours.

a 23% increase in the liquid and ice water path in the city sector. This difference between the URB and NOURB ensembles remains positive throughout the day, indicating that more water is available over the Paris city sector, which in this case leads to

an increase in precipitation.

5 | CONCLUSION

This study investigates the impact of densely urbanised areas on a convective precipitation event in the Paris region. The main contribution of this work lies in the use of an ensemble based on the AROME-EPS forecast system to simulate a specific convective situation and account for all associated uncertainties in weather modelling. This ensemble provided initial and lateral boundary conditions for the Meso-NH research model. To assess the impact of the urbanisation on precipitation, two sets of simulations at 300 m horizontal resolution were performed. One set used the TEB urban multi-layer scheme (URB), with a detailed description of urban surfaces. The other one replaced the urban surfaces with the predominant vegetation in the Paris region.

Comparisons with observations show a high variability within the ensemble for surface variables such as temperature, almost 22°C for the warmest member against 16°C for the coldest one in the afternoon, specific humidity (between 6.5 and 9 g kg^{-1} at 12 UTC), and for precipitation accumulation. In this experiment, the ensemble has a tendency to simulate too much precipitation and too early in the afternoon (Figure 4d), but nevertheless some members were able to simulate the initiation of convection over Paris quite accurately, like the member 1 or member 12 (Figure 8). In general, the comparison between the URB and NOURB ensembles shows a significant difference in precipitation accumulation. To complete the analysis, 7 sectors were defined in and around the Paris region to locate the area most affected by precipitation and to analyse the different processes involved. In the city sector, rainfall accumulation is increased by about 0.8 mm on average. This represents an increase of 70% for the URB ensemble compared to the NOURB ensemble. The application of the Wilcoxon t-test method confirms the significant increase in precipitation over the Paris city sector, while no clear difference is shown for the other sectors, except for a slight increase in the downwind left sector in the URB ensemble.

Warmer temperatures and drier conditions were simulated in the Paris region for the URB ensemble, especially in the city sector. They implied a higher sensible heat flux and a lower latent heat flux in the urban environment. The higher values of the sensible heat flux for the URB ensemble in the afternoon enhanced the vertical velocities above Paris and the development of the boundary layer. The results show an increase of about 5% of the updrafts over the city sector for the URB ensemble. The boundary layer is found to be on average 200 to 300 m higher in the URB ensemble (compared to the NOURB ensemble) and up to 700 m higher for the URB ensemble in the afternoon in the city centre. This increase in vertical velocity and boundary layer height leads to more clouds over the city, with almost 5% more clouds for the URB ensemble. The higher rainfall accumulation is associated with an increase of more than 20% in the total (liquid and ice) water path over Paris, leading to more ice and liquid water available over the capital. The robustness of the results is confirmed by an analysis of the other sectors, where no real trend of precipitation modification is found and no significant differences between the two ensembles are found for the variables mentioned.

This study provides a clear understanding of how urban surfaces can affect the lower and upper levels of the atmosphere in a diurnal convective environment with light flow and no large-scale interactions. It confirms the previous studies with an apparent effect of dense urbanisation on precipitation accumulation, in particular an increase of rainfall over the city (Bornstein and Lin, 2000; Liu and Niyogi, 2019). Although the ensemble tended to overestimate precipitation accumulation in most of the members in the 7 May case, statistical tests showed that despite the high variability of the ensemble, a significant increase in precipitation over the urban environment was found and could be attributed to the urbanised areas.

To further consolidate the results, it would be interesting to investigate other cases in the future, using the same ensemble approach, which clearly helps to discriminate a random effect from a real trend. The next step is to identify typical weather situations in which a modification of the convection caused by the Paris region can be expected. Interesting convective situations

would be for example cold fronts, night storms, or deep organised convection. Another perspective of this study is the evaluation of the modelling resolution effect on the ability of the ensemble forecasts to reproduce the city effect on precipitations. The methodology presented in this paper could also be applied to other cities around the world with different climates, locations (coastal city or city surrounded by mountains) and morphologies.

ACKNOWLEDGEMENTS

This work is a contribution to the Resarch and Demonstration Project Paris 2024 olympics in order to advance meteorological research on the theme of the "future Weather Forecasting systems at 100m (or finer) resolution for urban areas" supported by WMO. We wish to particularly thank Robert Schoetter and Jean Wurtz for valuable discussions on the Meso-NH model and the TEB urban scheme.

CONFLICTS OF INTEREST

The authors declare they have no conflicts of interest.

REFERENCES

Janet Barlow, Martin Best, Sylvia I. Bohnenstengel, Peter Clark, Sue Grimmond, Humphrey Lean, Andreas Christen, Stefan Emeis, Martial Haeffelin, Ian N. Harman, Aude Lemonsu, Alberto Martilli, Eric Pardyjak, Mathias W. Rotach, Susan Ballard, Ian Boutle, Andy Brown, Xiaoming Cai, Matteo Carpentieri, Omduth Coceal, Ben Crawford, Silvana Di Sabatino, Junxia Dou, Daniel R. Drew, John M. Edwards, Joachim Fallmann, Krzysztof Fortuniak, Jemma Gornall, Tobias Gronemeier, Christos H. Halios, Denise Hertwig, Kohin Hirano, Albert A. M. Holtslag, Zhiwen Luo, Gerald Mills, Makoto Nakayoshi, Kathy Pain, K. Heinke Schlünzen, Stefan Smith, Lionel Soulhac, Gert-Jan Steeneveld, Ting Sun, Natalie E. Theeuwes, David Thomson, James A. Voogt, Helen C. Ward, Zheng-Tong Xie, and Jian Zhong. Developing a Research Strategy to Better Understand, Observe, and Simulate Urban Atmospheric Processes at Kilometer to Subkilometer Scales. *Bulletin of the American Meteorological Society*, 98(10):ES261 – ES264, 2017. doi: 10.1175/BAMS-D-17-0106.1. URL https://journals.ametsoc.org/view/journals/bams/98/10/bams-d-17-0106.1.xml. Place: Boston MA, USA Publisher: American Meteorological Society.

J. Berner, S.-Y. Ha, J. P. Hacker, A. Fournier, and C. Snyder. Model uncertainty in a mesoscale ensemble prediction system: Stochastic versus multiphysics representations. *Monthly Weather Review*, 139(6):1972 – 1995, 2011. doi: 10.1175/2010MWR3595.1. URL https://journals.ametsoc.org/view/journals/mwre/139/6/2010mwr3595.1.xml.

Erwan Bocher, Jérémy Bernard, Elisabeth Le Saux Wiederhold, François Leconte, Gwendall Petit, Sylvain Palominos, and Camille Noûs. GeoClimate: a Geospatial processing toolbox for environmental and climate studies. *Journal of Open Source Software*, 6(65):3541, September 2021. doi: 10.21105/joss.03541. URL https://shs.hal.science/halshs-03359757.

A. Boone, V. Masson, T. Meyers, and J. Noilhan. The influence of the inclusion of soil freezing on simulations by a soil–vegetation–atmosphere transfer scheme. *Journal of Applied Meteorology*, 39(9):1544 – 1569, 2000. doi: 10.1175/1520-0450(2000)039<1544:TIOTIO>2.0.CO;2. URL https://journals.ametsoc.org/view/journals/apme/39/9/1520-0450_2000_039_1544_tiotio_2.0.co_2.xml.

R. Bornstein and Qinglu Lin. Urban heat islands and summertime convective thunderstorms in atlanta: three case studies. *Atmospheric Environment*, 34:507–516, 2000.

François Bouttier and Laure Raynaud. Clustering and selection of boundary conditions for limited-area ensemble prediction. *Quarterly Journal of the Royal Meteorological Society*, 144(717):2381–2391, 2018. doi: https://doi.org/10.1002/qj.3304. URL https://rmets.onlinelibrary.wiley.com/doi/abs/10.1002/qj.3304.

François Bouttier, Benoît Vié, Olivier Nuissier, and Laure Raynaud. Impact of stochastic physics in a convection-permitting ensemble. *Monthly Weather Review*, 140(11):3706 – 3721, 2012. doi: 10.1175/MWR-D-12-00031.1. URL https://journals.ametsoc.org/view/journals/mwre/140/11/mwr-d-12-00031.1.xml.

François Bouttier, Laure Raynaud, Olivier Nuissier, and Benjamin Ménétrier. Sensitivity of the arome ensemble to initial and surface perturbations during hymex. *Quarterly Journal of the Royal Meteorological Society*, 142(S1):390–403, 2016. doi: https://doi.org/10.1002/qj.2622. URL https://rmets.onlinelibrary.wiley.com/doi/abs/10.1002/qj.2622.

Pierre Brousseau, Yann Seity, Didier Ricard, and Julien Léger. Improvement of the forecast of convective activity from the arome-france system. *Quarterly Journal of the Royal Meteorological Society*, 142(699):2231–2243, 2016. doi: https://doi.org/10.1002/qj.2822. URL https://rmets.onlinelibrary.wiley.com/doi/abs/10.1002/qj.2822.

Stéphane Bélair, Sylvie Leroyer, Naoko SEINO, Lubos SPACEK, Vanh SOUVANLASSY, and Danahé Paquin-Ricard. Role and impact of the urban environment in a numerical forecast of an intense summertime precipitation event over tokyo. *Journal of the Meteorological Society of Japan. Ser. II*, 96A, 01 2018. doi: 10.2151/jmsj.2018-011.

G. Caniaux, J-L. Redelsperger, and J-P. Lafore. A numerical study of the stratiform region of a fast-moving squall line. part i: General description and water and heat budgets. *Journal of Atmospheric Sciences*, 51(14):2046 – 2074, 1994. doi: 10.1175/1520-0469(1994)051<2046:ANSOTS>2.0.CO;2. URL https://journals.ametsoc.org/view/journals/atsc/51/14/1520-0469_1994_051_2046_ansots_2_0_co_2.xml.

F. A. Huff P. T. Schickedanz Changnon, S. A. and J. L. Vogel. *Summary of METROMEX*, volume 1. Illinois State Water Survey, 1977.

H. Charnock. Wind stress on a water surface. *Quarterly Journal of the Royal Meteorological Society*, 81(350):639–640, 1955. doi: https://doi.org/10.1002/qj.49708135027. URL https://rmets.onlinelibrary.wiley.com/doi/abs/10.1002/qj.49708135027.

Fei Chen, Shiguang Miao, Mukul Tewari, Jian-Wen Bao, and Hiroyuki Kusaka. A numerical study of interactions between surface forcing and sea breeze circulations and their effects on stagnation in the greater houston area. *Journal of Geophysical Research: Atmospheres*, 116(D12), 2011. doi: https://doi.org/10.1029/2010JD015533. URL https://agupubs.onlinelibrary.wiley.com/doi/abs/10.1029/2010JD015533.

Sylvain Coquillat, Marie-Pierre Boussaton, Magalie Buguet, Dominique Lambert, Jean-François Ribaud, and Andy Berthelot. Lightning ground flash patterns over Paris aera between 1992 and 2003: influence of pollution. *Atmospheric Research*, 2012. doi: 10.1016/j.atmosres.2012.10.032. URL https://hal.archives-ouvertes.fr/hal-00766941.

J. Cuxart, P. Bougeault, and J.-L. Redelsperger. A turbulence scheme allowing for mesoscale and large-eddy simulations. *Quarterly Journal of the Royal Meteorological Society*, 126(562):1–30, 2000. doi: https://doi.org/10.1002/qj.49712656202. URL https://rmets.onlinelibrary.wiley.com/doi/abs/10.1002/qj.49712656202.

Thibaut Dauhut, Jean-Pierre Chaboureau, Juan Escobar, and Patrick Mascart. Large-eddy simulations of hector the convector making the stratosphere wetter. *Atmospheric Science Letters*, 16(2):135–140, 2015. doi: https://doi.org/10.1002/asl2.534. URL https://rmets.onlinelibrary.wiley.com/doi/abs/10.1002/asl2.534.

B. Decharme, A. Boone, C. Delire, and J. Noilhan. Local evaluation of the interaction between soil biosphere atmosphere soil multilayer diffusion scheme using four pedotransfer functions. *Journal of Geophysical Research: Atmospheres*, 116(D20), 2011. doi: https://doi.org/10.1029/2011JD016002. URL https://agupubs.onlinelibrary.wiley.com/doi/abs/10.1029/2011JD016002.

L. Descamps, C. Labadie, A. Joly, E. Bazile, P. Arbogast, and P. Cébron. Pearp, the météo-france short-range ensemble prediction system. *Quarterly Journal of the Royal Meteorological Society*, 141(690):1671–1685, 2014. doi: https://doi.org/10.1002/qj.2469. URL https://rmets.onlinelibrary.wiley.com/doi/abs/10.1002/qj.2469.

I. Douglas. *The Urban Environment*. Edward Arnold, 1983. ISBN 9780713163926. URL https://books.google.fr/books?id=KgZhQgAACAAJ.

Bradley Efron and Robert J. Tibshirani. *An Introduction to the Bootstrap*. Number 57 in Monographs on Statistics and Applied Probability. Chapman & Hall/CRC, Boca Raton, Florida, USA, 1993.

C. W. Fairall, E. F. Bradley, J. E. Hare, A. A. Grachev, and J. B. Edson. Bulk parameterization of air–sea fluxes: Updates and verification for the coare algorithm. *Journal of Climate*, 16(4):571 – 591, 2003. doi: 10.1175/1520-0442(2003)016<0571:BPOASF>2.0.CO;2. URL https://journals.ametsoc.org/view/journals/clim/16/4/1520-0442_2003_016_0571_bpoasf_2.0.co_2.xml.

R. Falga and C. Wang. Impact of urban land use on mean and heavy rainfall during the indian summer monsoon. *Atmospheric Chemistry and Physics*, 24(1):631–647, 2024. doi: 10.5194/acp-24-631-2024. URL https://acp.copernicus.org/articles/24/631/2024/.

J. Figueras i Ventura and Pierre Tabary. The new french operational polarimetric radar rainfall rate product. *Journal of Applied Meteorology and Climatology*, 52(8):1817 – 1835, 2013. doi: 10.1175/JAMC-D-12-0179.1. URL https://journals.ametsoc.org/view/journals/apme/52/8/jamc-d-12-0179.1.xml.

Y. Fouquart and B. Bonnel. Computations of solar heating of the earth's atmosphere: a new parameterization. *Beiträge zur Physik der Atmosphäre*, 53:35–62, 1980.

Inger-Lise Frogner, Andrew T. Singleton, Morten Ø. Køltzow, and Ulf Andrae. Convection-permitting ensembles: Challenges related to their design and use. *Quarterly Journal of the Royal Meteorological Society*, 145(S1):90–106, 2019. doi: https://doi.org/10.1002/qj.3525. URL https://rmets.onlinelibrary.wiley.com/doi/abs/10.1002/qj.3525.

T. Gal-Chen and Richard C.J Somerville. On the use of a coordinate transformation for the solution of the navier-stokes equations. *Journal of Computational Physics*, 17(2):209–228, 1975. ISSN 0021-9991. doi: https://doi.org/10.1016/0021-9991(75)90037-6. URL https://www.sciencedirect.com/science/article/pii/0021999175900376.

Nancy Grimm, Stanley Faeth, Nancy Golubiewski, Charles Redman, Jianguo Wu, Xuemei Bai, and John Briggs. Global change and the ecology of cities. *Science (New York, N.Y.)*, 319:756–60, 03 2008. doi: 10.1126/science.1150195.

Xueliang Guo, Danhong Fu, and Jing Wang. Mesoscale convective precipitation system modified by urbanization in beijing city. *Atmospheric Research*, 82(1):112–126, 2006. ISSN 0169-8095. doi: https://doi.org/10.1016/j.atmosres.2005.12.007. URL https://www.sciencedirect.com/science/article/pii/S0169809506000299. 14th International Conference on Clouds and Precipitation.

K. D. Hage. Urban-rural humidity differences. *Journal of Applied Meteorology*, 14:1277–1283, 1975. ISSN 0021-8952. doi: 10.1175/1520-0450(1975)014<1277:urhd>2.0.co;2.

Susanna Hagelin, Joohyung Son, Richard Swinbank, Anne McCabe, Nigel Roberts, and Warren Tennant. The met office convective-scale ensemble, mogreps-uk. *Quarterly Journal of the Royal Meteorological Society*, 143(708):2846–2861, 2017. doi: https://doi.org/10.1002/qj.3135. URL https://rmets.onlinelibrary.wiley.com/doi/abs/10.1002/qj.3135.

Julia Hidalgo, Aude Lemonsu, and Valéry Masson. Between progress and obstacles in urban climate interdisciplinary studies and knowledge transfer to society: Urban climate interdisciplinary studies. *Annals of the New York Academy of Sciences*, 1436, 11 2018. doi: 10.1111/nyas.13986.

Rachel Honnert, Georgios A. Efstathiou, Robert J. Beare, Junshi Ito, Adrian Lock, Roel Neggers, Robert S. Plant, Hyeyum Hailey Shin, Lorenzo Tomassini, and Bowen Zhou. The atmospheric boundary layer and the "gray zone" of turbulence: A critical review. *Journal of Geophysical Research: Atmospheres*, 125(13):e2019JD030317, 2020. doi: https://doi.org/10.1029/2019JD030317. URL https://agupubs.onlinelibrary.wiley.com/doi/abs/10.1029/2019JD030317. e2019JD030317 10.1029/2019JD030317.

Rachel Honnert, Valéry Masson, Christine Lac, and Tim Nagel. A Theoretical Analysis of Mixing Length for Atmospheric Models From Micro to Large Scales. *Frontiers in Earth Science*, 8:582056, 2021. doi: 10.3389/feart.2020.582056. URL https://hal-meteofrance.archives-ouvertes.fr/meteo-03357801.

ROBERT E. Horton. Thunderstorm-breeding spots. *Monthly Weather Review*, 49(4):193 – 193, 1921. doi: https://doi.org/10.1175/1520-0493(1921)49<193a:TS>2.0.CO;2. URL https://journals.ametsoc.org/view/journals/mwre/49/4/1520-0493_1921_49_193a_ts_2_0_co_2.xml.

F. A. Huff and S. A. Changnon. precipitation modification by major urban areas. *Bulletin of the American Meteorological Society*, 54(12):1220–1232, 1973. ISSN 00030007, 15200477. URL http://www.jstor.org/stable/26255213.

Darrel M. Kingfield, Kristin M. Calhoun, Kirsten M. de Beurs, and Geoffrey M. Henebry. Effects of city size on thunderstorm evolution revealed through a multiradar climatology of the central united states. *Journal of Applied Meteorology and Climatology*, 57(2):295 – 317, 2018. doi: 10.1175/JAMC-D-16-0341.1. URL https://journals.ametsoc.org/view/journals/apme/57/2/jamc-d-16-0341.1.xml.

C. Lac, J.-P. Chaboureau, V. Masson, J.-P. Pinty, P. Tulet, J. Escobar, M. Leriche, C. Barthe, B. Aouizerats, C. Augros, P. Aumond, F. Auguste, P. Bechtold, S. Berthet, S. Bielli, F. Bosseur, O. Caumont, J.-M. Cohard, J. Colin, F. Couvreux, J. Cuxart, G. Delautier, T. Dauhut, V. Ducrocq, J.-B. Filippi, D. Gazen, O. Geoffroy, F. Gheusi, R. Honnert, J.-P. Lafore, C. Lebeaupin Brossier, Q. Libois, T. Lunet, C. Mari, T. Maric, P. Mascart, M. Mogé, G. Molinié, O. Nuissier, F. Pantillon, P. Peyrillé, J. Pergaud, E. Perraud, J. Pianezze, J.-L. Redelsperger, D. Ricard, E. Richard, S. Riette, Q. Rodier, R. Schoetter, L. Seyfried, J. Stein, K. Suhre, M. Taufour, O. Thouron, S. Turner, A. Verrelle, B. Vié, F. Visentin, V. Vionnet, and P. Wautelet. Overview of the meso-nh model version 5.4 and its applications. *Geoscientific Model Development*, 11(5):1929–1969, 2018. doi: 10.5194/gmd-11-1929-2018. URL https://gmd.copernicus.org/articles/11/1929/2018/.

O. Laurantin. ANTILOPE: hourly rainfall analysis over France merging radar and rain gauges data. In *Proceedings of the 11th International Precipitation Conference*, 2013.

Benjamin Le Roy, Aude Lemonsu, Raphaëlle Kounkoud-Arnaud, Denis Brion, and Valéry Masson. Long time series spatialized data for urban climatological studies: a case study of Paris, France Long time series spatialized data for urban climatological studies. *International Journal of Climatology*, November 2020. doi: 10.1002/joc.6414. URL https://hal.archives-ouvertes.fr/hal-02391035.

Aude Lemonsu and Valéry Masson. Simulation of a summer urban breeze over paris. *Boundary-Layer Meteorology*, 104:463–490, 01 2002. doi: 10.1023/A:1016509614936.

Sylvie Leroyer, Stéphane Bélair, Syed Husain, and Jocelyn Mailhot. Subkilometer numerical weather prediction in an urban coastal area: A case study over the vancouver metropolitan area. *Journal of Applied Meteorology and Climatology*, 53:1433–1453, 06 2014. doi: 10.1175/JAMC-D-13-0202.1.

Jie Liu and Dev Niyogi. Meta-analysis of urbanization impact on rainfall modification. *Scientific Reports*, 9(1):7301, May 2019. ISSN 2045-2322. doi: 10.1038/s41598-019-42494-2. URL https://doi.org/10.1038/s41598-019-42494-2.

Judith M. Lorenz, Rico Kronenberg, Christian Bernhofer, and Dev Niyogi. Urban rainfall modification: Observational climatology over berlin, germany. *Journal of Geophysical Research: Atmospheres*, 124(2):731–746, 2019. doi: https://doi.org/10.1029/2018JD028858. URL https://agupubs.onlinelibrary.wiley.com/doi/abs/10.1029/2018JD028858.

Jean F. Louis. A parametric model of vertical eddy fluxes in the atmosphere. *Boundary-Layer Meteorology*, 17:187–202, 1979.

Thibaut Lunet, C. Lac, Auguste Franck, Florian Visentin, Valéry Masson, and Juan Escobar. Combination of weno and explicit runge-kutta methods for wind transport in meso-nh model. *Monthly Weather Review*, 145, 07 2017. doi: 10.1175/MWR-D-16-0343.1.

Yali Luo, Jiahua Zhang, Miao Yu, Xudong Liang, Rudi Xia, Yanyu Gao, Xiaoyu Gao, and Jinfang Yin. On the influences of urbanization on the extreme rainfall over zhengzhou on 20 july 2021: A convection-permitting ensemble modeling study. 40(3):393–409, 2022. doi: 10.1007/s00376-022-2048-8.

M. Mandement and O. Caumont. A numerical study to investigate the roles of former hurricane leslie, orography and evaporative cooling in the 2018 aude heavy-precipitation event. *Weather and Climate Dynamics*, 2(3):795–818, 2021. doi: 10.5194/wcd-2-795-2021. URL https://wcd.copernicus.org/articles/2/795/2021/.

Iris Manola, Gert-Jan Steeneveld, Remko Uijlenhoet, and Albert A. M. Holtslag. Analysis of urban rainfall from hourly to seasonal scales using high-resolution radar observations in the netherlands. *International Journal of Climatology*, 40(2):822–840, 2020. doi: https://doi.org/10.1002/joc.6241. URL https://rmets.onlinelibrary.wiley.com/doi/abs/10.1002/joc.6241.

Paul Markowski and Yvette Richardson. *Mesoscale Meteorology in Midlatitudes*. Wiley-Blackwell, 2010. ISBN 9780470682104.

V. Masson, P. Le Moigne, E. Martin, S. Faroux, A. Alias, R. Alkama, S. Belamari, A. Barbu, A. Boone, F. Bouyssel, P. Brousseau, E. Brun, J.-C. Calvet, D. Carrer, B. Decharme, C. Delire, S. Donier, K. Essaouini, A.-L. Gibelin, H. Giordani, F. Habets, M. Jidane, G. Kerdraon, E. Kourzeneva, M. Lafaysse, S. Lafont, C. Lebeaupin Brossier, A. Lemonsu, J.-F. Mahfouf, P. Marguinaud, M. Mokhtari, S. Morin, G. Pigeon, R. Salgado, Y. Seity, F. Taillefer, G. Tanguy, P. Tulet, B. Vincendon, V. Vionnet, and A. Voldoire. The surfexv7.2 land and ocean surface platform for coupled or offline simulation of earth surface variables and fluxes. *Geoscientific Model Development*, 6(4): 929–960, 2013. doi: 10.5194/gmd-6-929-2013. URL https://gmd.copernicus.org/articles/6/929/2013/.

Valéry Masson. A physically-based scheme for the urban energy budget in atmospheric models. *Boundary-Layer Meteorology*, 94: 357–397, 01 2000. doi: 10.1023/A:1002463829265.

Valéry Masson, Jean-Louis Champeaux, Fabrice Chauvin, Christelle Meriguet, and Roselyne Lacaze. A global database of land surface parameters at 1-km resolution in meteorological and climate models. *Journal of Climate*, 16(9):1261 – 1282, 2003. doi: 10.1175/1520-0442(2003)16<1261:AGDOLS>2.0.CO;2. URL https://journals.ametsoc.org/view/journals/clim/16/9/1520-0442_2003_16_1261_agdols_2.0.co_2.xml.

Valéry Masson, Aude Lemonsu, Julia Hidalgo, and James Voogt. Urban Climates and Climate Change. *Annual Review of Environment and Resources*, 45(1):411–444, 2020. doi: 10.1146/annurev-environ-012320-083623. URL https://doi.org/10.1146/annurev-environ-012320-083623. _eprint: https://doi.org/10.1146/annurev-environ-012320-083623.

Eli J. Mlawer, Steven J. Taubman, Patrick D. Brown, Michael J. Iacono, and Shepard A. Clough. Radiative transfer for inhomogeneous atmospheres: Rrtm, a validated correlated-k model for the longwave. *Journal of Geophysical Research: Atmospheres*, 102(D14): 16663–16682, 1997. doi: https://doi.org/10.1029/97JD00237. URL https://agupubs.onlinelibrary.wiley.com/doi/abs/10.1029/97JD00237.

Dev Niyogi, Teddy Holt, Sharon Zhong, Patrick C. Pyle, and Jeffery Basara. Urban and land surface effects on the 30 july 2003 mesoscale convective system event observed in the southern great plains. *Journal of Geophysical Research: Atmospheres*, 111(D19), 2006. doi: https://doi.org/10.1029/2005JD006746. URL https://agupubs.onlinelibrary.wiley.com/doi/abs/10.1029/2005JD006746.

Dev Niyogi, Patrick Pyle, Ming Lei, S. Pal Arya, Chandra M. Kishtawal, Marshall Shepherd, Fei Chen, and Brian Wolfe. Urban modification of thunderstorms: An observational storm climatology and model case study for the indianapolis urban region. *Journal of Applied Meteorology and Climatology*, 50(5):1129 – 1144, 2011. doi: 10.1175/2010JAMC1836.1. URL https://journals.ametsoc.org/view/journals/apme/50/5/2010jamc1836.1.xml.

O. Nuissier, F. Duffourg, M. Martinet, V. Ducrocq, and C. Lac. Hectometric-scale simulations of a mediterranean heavy-precipitation event during the hydrological cycle in the mediterranean experiment (hymex) first special observation period (sop1). *Atmospheric Chemistry and Physics*, 20(23):14649–14667, 2020. doi: 10.5194/acp-20-14649-2020. URL https://acp.copernicus.org/articles/20/14649/2020/.

T. Oke. City size and the urban heat island. *Atmospheric Environment (1967)*, 7:769–779, 08 1973. doi: 10.1016/0004-6981(73)90140-6.

OpenStreetMap. Données openstreetmap, 2021. URL https://www.openstreetmap.org.

Julien Pergaud, Valéry Masson, Sylvie Malardel, and F. Couvreux. A parameterization of dry thermals and shallow cumuli for mesoscale numerical weather prediction. *Boundary-Layer Meteorology*, 132:83–106, 07 2009. doi: 10.1007/s10546-009-9388-0.

Jean-Pierre Pinty and Patrick Jabouille. A mixed-phase cloud parameterization for use in a mesoscale non-hydrostatic model: Simulations of a squall line of orographic precipitation. In *in: Proceedings of the Conference of Cloud Physics 17–21 August 1998*, pages 217–220, Boston MA, USA, 1998. American Meteorological Society.

V.S. Platonov, M.I. Varentsov, Yu.I. Yarinich, A.N. Shikhov, and A.V. Chernokulsky. A large mid-latitude city intensifies severe convective events: Evidence from long-term high-resolution simulations. *Urban Climate*, 54:101837, 2024. ISSN 2212-0955. doi: https://doi.org/10.1016/j.uclim.2024.101837. URL https://www.sciencedirect.com/science/article/pii/S2212095524000336.

Laure Raynaud and F. Bouttier. Comparison of initial perturbation methods for ensemble prediction at convective scale. *Quarterly Journal of the Royal Meteorological Society*, 142:n/a–n/a, 10 2015. doi: 10.1002/qj.2686.

RDP. Research demonstration project paris 2024 olympics, 2020. URL http://www.umr-cnrm.fr/RDP_Paris2024.

H. Richardson, Sukanta Basu, and Bert Holtslag. Improving stable boundary-layer height estimation using a stability-dependent critical bulk richardson number. *Boundary-Layer Meteorology*, 148, 07 2013. doi: 10.1007/s10546-013-9812-3.

Quentin Rodier, Valéry Masson, F. Couvreux, and Alexandre Paci. Evaluation of a buoyancy and shear based mixing length for a turbulence scheme. *Frontiers in Earth Science*, 5:65, 08 2017. doi: 10.3389/feart.2017.00065.

Christopher M. Rozoff, William R. Cotton, and Jimmy O. Adegoke. Simulation of st. louis, missouri, land use impacts on thunderstorms. *Journal of Applied Meteorology*, 42(6):716 – 738, 2003. doi: https://doi.org/10.1175/1520-0450(2003)042<0716:SOSLML>2.0.CO;2. URL https://journals.ametsoc.org/view/journals/apme/42/6/1520-0450_2003_042_0716_soslml_2.0.co_2.xml.

Young-Hee Ryu, James A. Smith, Elie Bou-Zeid, and Mary L. Baeck. The influence of land surface heterogeneities on heavy convective rainfall in the baltimore–washington metropolitan area. *Monthly Weather Review*, 144(2):553 – 573, 2016. doi: https://doi.org/10.1175/MWR-D-15-0192.1. URL https://journals.ametsoc.org/view/journals/mwre/144/2/mwr-d-15-0192.1.xml.

R. Schoetter, Y. T. Kwok, C. de Munck, K. K. L. Lau, W. K. Wong, and V. Masson. Multi-layer coupling between surfex-teb-v9.0 and meso-nh-v5.3 for modelling the urban climate of high-rise cities. *Geoscientific Model Development*, 13(11):5609–5643, 2020. doi: 10.5194/gmd-13-5609-2020. URL https://gmd.copernicus.org/articles/13/5609/2020/.

Y. Seity, P. Brousseau, S. Malardel, G. Hello, P. Bénard, F. Bouttier, C. Lac, and V. Masson. The arome-france convective-scale operational model. *Monthly Weather Review*, 139(3):976 – 991, 2011. doi: 10.1175/2010MWR3425.1. URL https://journals.ametsoc.org/view/journals/mwre/139/3/2010mwr3425.1.xml.

Willis Shem and Marshall Shepherd. On the impact of urbanization on summertime thunderstorms in atlanta: Two numerical model case studies. *Atmospheric Research - ATMOS RES*, 92:172–189, 04 2009. doi: 10.1016/j.atmosres.2008.09.013.

Hikari Shimadera, Akira Kondo, Kundan Shrestha, Ken Kitaoka, and Yoshio Inoue. Numerical evaluation of the impact of urbanization on summertime precipitation in osaka, japan. *Advances in Meteorology*, 2015, 06 2015. doi: 10.1155/2015/379361.

Chi-Wang Shu and Stanley Osher. Efficient implementation of essentially non-oscillatory shock-capturing schemes. *Journal of Computational Physics*, 77(2):439–471, 1988. ISSN 0021-9991. doi: https://doi.org/10.1016/0021-9991(88)90177-5. URL https://www.sciencedirect.com/science/article/pii/0021999188901775.

Xiaomeng Song, Jianyun Zhang, Amir AghaKouchak, Shouraseni Sen Roy, Yunqing Xuan, Guoqing Wang, Ruimin He, Xiaojun Wang, and Cuishan Liu. Rapid urbanization and changes in spatiotemporal characteristics of precipitation in beijing metropolitan area. *Journal of Geophysical Research: Atmospheres*, 119(19):11,250–11,271, 2014. doi: https://doi.org/10.1002/2014JD022084. URL https://agupubs.onlinelibrary.wiley.com/doi/abs/10.1002/2014JD022084.

I. D. Stewart and T. R. Oke. Local climate zones for urban temperature studies. *Bulletin of the American Meteorological Society*, 93(12):1879 – 1900, 2012. doi: 10.1175/BAMS-D-11-00019.1. URL https://journals.ametsoc.org/view/journals/bams/93/12/bams-d-11-00019.1.xml.

A. Christen J. A. Voogt T. R. Oke, G. Mills. *Urban Climate*. Cambdridge University Press, UK, 2017.

Jianguo Tan, Youfei Zheng, Xu Tang, Changyi Guo, Liping li, Guixiang Song, Xinrong Zhen, Dong Yuan, Adam Kalkstein, and Furong Li. The urban heat island and its impact on heat waves and human health in shanghai. *International journal of biometeorology*, 54:75–84, 10 2009. doi: 10.1007/s00484-009-0256-x.

Ina Tegen, Peter Hollrig, Mian Chin, Inez Fung, Daniel Jacob, and Joyce Penner. Contribution of different aerosol species to the global aerosol extinction optical thickness: Estimates from model results. *Journal of Geophysical Research: Atmospheres*, 102(D20):23895–23915, 1997. doi: https://doi.org/10.1029/97JD01864. URL https://agupubs.onlinelibrary.wiley.com/doi/abs/10.1029/97JD01864.

Natalie Theeuwes, Janet Barlow, Adriaan Teuling, Christine Grimmond, and Simone Kotthaus. Persistent cloud cover over mega-cities linked to surface heat release. *npj Climate and Atmospheric Science*, 2, 05 2019. doi: 10.1038/s41612-019-0072-x.

UN. *World Population Prospects 2022: Summary of results*. United Nations Department of Economic and Social Affairs, 07 2022. ISBN 978-92-1-148373-4.

Mikhail Varentsov, Hendrik Wouters, Vladimir Platonov, and Pavel Konstantinov. Megacity-induced mesoclimatic effects in the lower atmosphere: A modeling study for multiple summers over moscow, russia. *Atmosphere*, 9(2), 2018. ISSN 2073-4433. doi: 10.3390/atmos9020050. URL https://www.mdpi.com/2073-4433/9/2/50.

Rong Wang and Raymond J. Spiteri. Linear instability of the fifth-order weno method. *SIAM Journal on Numerical Analysis*, 45(5): 1871–1901, 2007. ISSN 00361429. URL http://www.jstor.org/stable/40232807.

D.S. Wilks. *Statistical Methods in the Atmospheric Sciences*. Number vol. 100 in International Geophysics. Elsevier Science, 2006. ISBN 9780127519661. URL https://books.google.fr/books?id=_vSwyt8_OGEC.

Earle R. Williams, Daniel Rosenfeld, Nadia Madden, C. Labrada, John C. Gerlach, and L. Atkinson. The role of boundary layer aerosol in the vertical development of precipitation and electrification: Another look at the contrast between lightning over land and over ocean. 1999.

Wei Zhang, Gabriele Villarini, Gabriel Vecchi, and James Smith. Urbanization exacerbated the rainfall and flooding caused by hurricane harvey in houston. *Nature*, 563, 11 2018. doi: 10.1038/s41586-018-0676-z.

Shi Zhong and Xiu-Qun Yang. Ensemble simulations of the urban effect on a summer rainfall event in the great beijing metropolitan area. *Atmospheric Research*, 153:318–334, 2015. ISSN 0169-8095. doi: https://doi.org/10.1016/j.atmosres.2014.09.005. URL https://www.sciencedirect.com/science/article/pii/S0169809514003627.